


RESEARCH

Open Access



Long-term exercise enhances meningeal lymphatic vessel plasticity and drainage in a mouse model of Alzheimer's disease

Yan Chen^{1,2}, Jiachen Cai¹, Yuzhu She¹, Xiaoxin He¹, Hu Feng¹, Xuwei Li², Yiran Wei², Yi Fan³, Wen-e Zhao⁴, Mengmei Yin^{1,5}, Linjuan Yuan¹, Yuxi Jin¹, Fengfei Ding⁶, Chengyu Sheng¹, Junying Gao^{1,7*}, Qian Li^{1*} and Ming Xiao^{1,3*} 

Abstract

Background Meningeal lymphatic drainage is crucial for the clearance of amyloid β (A β), supporting the maintenance of brain homeostasis. This makes it a promising therapeutic target for Alzheimer's disease (AD). Long-term exercise can reduce the risk of AD; however, the underlying mechanism is not fully understood. In this study, we investigated whether exercise alleviates AD-related pathological changes by improving meningeal lymphatic drainage and its potential mechanisms.

Methods The morphological and functional features of meningeal lymphatic vessels, as well as A β and reactive gliosis in the brain, were compared between 6.5-month-old 5 \times FAD mice with or without 1 month of treadmill exercise. RNA sequencing, protein interactions analysis, gene knockdown mediated by adeno-associated virus, and lymphatic endothelial cell culture were conducted to investigate the mechanism underlying exercise-induced meningeal lymphatic vessel plasticity in 5 \times FAD mice.

Results The structural integrity of meningeal lymphatic vessels was compromised in 5 \times FAD mice, compared with the wild-type mice. Treadmill exercise increased the diameter and the drainage capacity of the meningeal lymphatic vessels, reduced A β deposition, reactive gliosis and astrocyte senescence in the hippocampus and frontal cortex, and improved cognitive function of 5 \times FAD mice. Mechanistically, thrombospondin-1 (TSP-1) exacerbated the inhibitory effect of A β on lymphatic vessel formation and plasticity through interactions with CD36 and CD47, respectively. Exercise decreased the expression of TSP-1 in reactive astrocytes of AD mice by downregulating eleven-nineteen lysine-rich leukemia-associated factor 2 (EAF2), a protein that facilitates the transcription of the TSP-1-encoding gene *Thbs-1* by binding p53. Ultimately, we found that hippocampal astrocyte-specific knockdown of *Thbs-1* or *Eaf2* enhanced meningeal lymphatic drainage and alleviated AD-like pathology in the hippocampus of 5 \times FAD mice.

[†]Yan Chen and Jiachen Cai have contributed equally to this work.

*Correspondence:

Junying Gao
gaojunying@njmu.edu.cn
Qian Li
liqian2019@njmu.edu.cn
Ming Xiao
mingx@njmu.edu.cn

Full list of author information is available at the end of the article



© The Author(s) 2025. **Open Access** This article is licensed under a Creative Commons Attribution 4.0 International License, which permits use, sharing, adaptation, distribution and reproduction in any medium or format, as long as you give appropriate credit to the original author(s) and the source, provide a link to the Creative Commons licence, and indicate if changes were made. The images or other third party material in this article are included in the article's Creative Commons licence, unless indicated otherwise in a credit line to the material. If material is not included in the article's Creative Commons licence and your intended use is not permitted by statutory regulation or exceeds the permitted use, you will need to obtain permission directly from the copyright holder. To view a copy of this licence, visit <http://creativecommons.org/licenses/by/4.0/>. The Creative Commons Public Domain Dedication waiver (<http://creativecommons.org/publicdomain/zero/1.0/>) applies to the data made available in this article, unless otherwise stated in a credit line to the data.

Conclusions Long-term exercise protects against AD by enhancing the plasticity and drainage of meningeal lymphatic vessels through downregulation of the EAF2–p53–TSP-1 pathway associated with reactive astrocytes.

Keywords Alzheimer's disease, Lymphangiogenesis, Meningeal lymphatics, Treadmill exercise, EAF2-p53-TSP-1

Introduction

Alzheimer's disease (AD) is one of the most common age-dependent neurodegenerative diseases, posing a serious threat to the health and life of older adults. Although monoclonal antibodies such as aducanumab and lecanemab can specifically reduce the deposition of amyloid β (A β) plaques, their long-term efficacy and potential complications still present challenges [1]. It is known that the imbalance between the production and clearance of A β occurs prior to the onset of cognitive impairment, causing excessive aggregation of A β and a series of neuropathological cascades [2]. Notably, a large number of astrocytes are persistently activated and undergo senescence, losing their ability to maintain brain homeostasis and exhibiting the senescence-associated secretory phenotype, which in turn accelerates neurodegeneration [3, 4]. Therefore, timely and effective clearance of A β from the brain and prevention of astrocyte senescence may be beneficial for delaying or even preventing the onset of AD [5, 6].

Meningeal lymphatic vessels have recently been characterized in humans and rodents [7]. They mediate the drainage of macromolecular waste [8, 9], cellular debris [10], neurotropic viruses [11], and brain tumor cells [12] from the brain. Meningeal lymphatic drainage progressively deteriorates during natural aging and in AD [13–15]. Blocking meningeal lymphatic vessels exacerbates A β load and memory deficits in transgenic mouse models of AD [8, 14]. Therefore, enhancing meningeal lymphatic drainage could be a novel therapeutic target for AD.

Notably, the specialized morphological features of meningeal lymphatic vessels are associated with their drainage functions [15]. A continuous zipper-like vascular endothelial (VE)–cadherin junction and a discontinuous button-like junctional pattern in lymphatic endothelial cells (LECs) are associated with distinct modes of cerebrospinal fluid (CSF) macromolecule transport facilitated by meningeal lymphatic vessels. Zipper-like junctions form tight, continuous barriers that support directional fluid flow, while button-like junctions are more permissive and facilitate macromolecule uptake. Balance between these junction types is crucial for efficient CSF drainage and is disrupted in aged mice, potentially contributing to impaired brain waste clearance [15]. Overexpression of vascular endothelial growth

factor C (VEGFC) induces meningeal lymphangiogenesis [16], whereas inhibitors of lymphangiogenesis, such as pigment epithelium-derived factor, suppress peripheral nasopharyngeal lymphangiogenesis [17]. Nonetheless, the mechanisms that underlie the impairment of the integrity and plasticity of meningeal lymphatic vessels during the progression of AD remain unclear.

Exercise intervention is one of the most effective non-pharmacologic therapeutic modalities, exerting beneficial effects on various organs, particularly the brain [18, 19]. For example, long-term exercise not only enhances the production of brain-derived neurotrophic factor [20] and synaptic plasticity [21], but also diminishes oxidative stress [22] and age-related gliosis [23] in the brain. Additionally, recent evidence suggests that the astrocytic aquaporin 4 (AQP4)-mediated glymphatic transport plays a role in the neuroprotective effects of voluntary exercise [24–26]. Nonetheless, it remains undetermined whether exercise can enhance meningeal lymphatic plasticity during the progression of AD.

Here, we investigated the role of astrocyte-derived factors in the regulation of meningeal lymphatic vessel function in a 5 \times FAD transgenic mouse model of AD. We further examined how long-term physical exercise influences astrocyte activity, meningeal lymphatic drainage, and A β clearance. By integrating genetic and behavioral interventions, our work aimed to identify novel astrocyte-derived modulators of lymphangiogenesis and to explore the therapeutic potential of exercise in ameliorating A β -associated neuropathology and cognitive impairment.

Methods

Animals

B6.Cg-Tg (APP^{SwF/Lon}, PSEN1^{*M146L*L286V}) 6799Vas/Mmjax (5 \times FAD, strain# 008730) mice were obtained from Jackson Laboratories (Bar Harbor, ME). The mice, along with their age-matched wild-type (WT) littermates, were housed in controlled ambient temperatures and exposed to a 12-h light/12-h dark cycle, with free access to standard rodent chow and clean water. Each group of mice consisted of equal numbers of males and females. All animal experiments were approved by the Animal Care and Use Committee of Nanjing Medical University (IACUC-1812054).

Treadmill exercise training

5×FAD mice aged 5.5 months were randomly assigned to either a treadmill exercise group or a sedentary group. The treadmill exercise was applied twice a day (at 09:00 and 20:00, respectively), for one month. Mice were acclimated and trained on a 10° uphill treadmill, beginning with 30 min of running at 8 m/min, followed by 30 min at 10 m/min for the first two days as a warm-up. Starting on the third day, mice were subjected to increasing treadmill speeds, with increments of 1 m/min every 20 min, for a total of 90 min per session [27]. Mice in the sedentary control group were kept in identical conditions but remained in their natural state. After one month of repeated training, the animals underwent behavioral tests followed by pathological analyses.

In vivo two-photon imaging

After 10 days of treadmill exercise training, mice were anesthetized with an intraperitoneal injection of a mixed ketamine (80 mg/kg) and xylazine (8 mg/kg) in saline, and secured in a stereotaxic device. The hair was shaved from head to neck and skin was cleaned with iodine and 75% ethanol. Following a surgical skin incision above the parietal region, the skull bone was thinned using an electrical micro drill. A total of 3 µL of A488-Lyve-1 (Invitrogen, Carlsbad, CA; Cat# 53-0443-82) was injected into the cisterna magna within 5 min via a 5 µL Hamilton syringe. The syringe was left in place for an additional 5 min and then withdrawn slowly. After suturing the exposed incision, the mice were returned to their home cage. Twenty-four hours later, they received an intrahippocampal injection (anteroposterior −2.0 mm, mediolateral ±1.8 mm, dorsoventral −2.0 mm) of 1 µL of Fluor 555-labeled Aβ (1 mg/mL, AnaSpec, Fremont, CA; Cat# AS-60480-01). One hour later, in vivo two-photon imaging was performed. Mouse head was fixed on a metal holder to minimize movement during live imaging. As previously described [11], a confocal scanning system (Zeiss ZEN) equipped with a two-photon laser scanning microscope and a 20× water-immersion lens installed on an upright microscope (Zeiss LSM880, Germany) was used for imaging.

AAV-mediated knockdown of *Thbs-1* or *Eaf2* in astrocytes

rAAV-GFaABC1D-mCherry-5' miR-30a-shRNA (*Thbs1*)-3' miR-30a-WPREs and rAAV-GFaABC1D-EGFP-5' miR-30a-shRNA (*Eaf2*)-3' miR-30a-WPREs were obtained from BrainVTA (Wuhan, China). The shRNA sequences verified to efficiently knockdown mouse *Thbs-1* or *Eaf2* were used: siRNA *Thbs1*, 5'-GAUGACUACGCUGGCUUUGUU-3', siRNA *Eaf2*, 5'-GGACUCCAAUCUUGUACATT-3'. As described above, after anesthetization, 5-month-old

WT and 5×FAD mice were secured in a stereotaxic apparatus. rAAV2/5-GFaABC1D-*Thbs1*-shRNA-mCherry, rAAV2/9-GFaABC1D-scramble-shRNA-mCherry, rAAV2/5-GFaABC1D-*Eaf2*-shRNA-EGFP, or rAAV2/5-GFaABC1D-scramble-shRNA-EGFP was injected into the bilateral hippocampal region (anteroposterior −2.0 mm, mediolateral ±1.8 mm, dorsoventral −2.0 mm, 1 µL for each hemisphere). Four weeks after virus injection, mouse behavior and pathology were evaluated.

Y-maze test

The Y maze (27 cm×9 cm×24 cm) consisted of three arms. During the training stage, each mouse was placed in the start arm to explore for 5 min, with the novel arm being blocked. Two hours later, the mouse was allowed to freely explore the entire maze for 5 min. The percentage of time spent in the novel arm and the number of entries into the novel arm were recorded by the video tracking software (TopScan, CleverSys, Inc., Reston, VA).

Novel object recognition (NOR) test

The NOR test was conducted in two phases: familiarization and testing [10]. During the familiarization phase, each animal was permitted to freely explore an open arena (40 cm×40 cm×30 cm) for 5 min, in which two identical objects were placed in opposite diagonal corners. In the testing phase 2 h later, one familiar object was replaced by a novel object (differing in color and shape), and the mice were allowed to explore the arena for another 5 min. Exploration of objects was defined as mouse sniffing or interacting with an object from within 2 cm and was quantified using a video tracking software (TopScan, CleverSys, Inc.). The discrimination index was calculated as follows: discrimination index = $(T_{\text{novel}} - T_{\text{familiar}}) / (T_{\text{novel}} + T_{\text{familiar}})$.

Elevated plus maze (EPM) test

The EPM consisted of two open arms (35 cm×6 cm) and two closed arms (35 cm×6 cm×15 cm), each elevated 75 cm above the floor. Mice were placed in the central hub and allowed to freely explore the maze for 5 min. A video tracking software (TopScan, CleverSys, Inc.) was utilized to quantify the time spent in the open arms and the frequency of entries into the open arms.

Primary astrocytes and cell line cultures and treatment

Primary astrocytes were isolated from neonatal mice as previously described [10]. In brief, after removing the meningeal vessels, the hippocampus and surrounding cortices were microdissected and subjected to trypsin digestion. Tissue homogenates were passed through a 70-µm mesh filter, resuspended in astrocyte growth

medium (DMEM (Gibco, Carlsbad, CA; Cat# 11960) containing 10% FBS and 100 U/mL penicillin/streptomycin (Gibco, Cat# 15–140-122), and plated on 10-cm petri dishes. The cells were incubated at 37 °C in 5% CO₂. The medium was fully replaced every 3 to 4 days, and cells were passaged using 0.05% Trypsin (Gibco, Cat# 25–200-056) when they reached full growth.

For experiments involving treatment of primary astrocytes with A β _{1–42} oligomers, primary astrocytes (12–15 days in vitro, DIV 12–15) were transferred to complete serum medium and then incubated in the presence or absence of oligomeric A β _{1–42} (at concentrations of 0, 5, and 10 μ mol/L) for 48 h. Some experiments continued with transfection of siR-Eaf2, after which the pellet and supernatant were collected 72 h later.

Cultures of the *Mus musculus* lymphoid endothelial cell line (SVEC4-10) (ATCC, Cat# CRL-2181), human aortic endothelial cells (HAECs) and human-derived lymphatic endothelial cell line (HLEC) were routinely maintained in DMEM medium supplemented with 10% FBS and 100 U/mL penicillin/streptomycin. The SVEC4-10 cells were planted on a 24-well plate and then treated with a gradient concentration of recombinant TSP-1 protein (R&D Systems, Minneapolis, MN; Cat# 3074-TH-050) or oligomer A β _{1–42}. To investigate the effect of the TSP-1–CD47 pathway on junctional patterns in vitro, SVEC4-10 cells were pretreated with siR-CD47 before treatment with recombinant TSP-1. The sequences were as follows:

siR-Eaf2, 5′-CAAAGGCUGCUCCAGCUCUdT₃′;

siR-Cd47 (Mus), 5′-CUUGCAUCGUCCGUAAUGUTT₃′;

Negative control (NC), 5′-UUCUCCGAACGUGUCACGUTT₃′.

CSF and tissue collection

After anesthesia, CSF was collected from the cisterna magna using a borosilicate glass pipette with an internal filament, and centrifuged at 1000 \times g for 15 min. The supernatant was carefully transferred to a collection tube and stored at –80 °C. Subsequently, the deep cervical lymph nodes (dCLNs) were removed and preserved in 4% paraformaldehyde (PFA). The mice were then transcardially perfused with ice-cold phosphate-buffered saline (PBS). Following the removal of the skin and muscle from the head, the hippocampi were collected and stored at –80 °C until further processing. The brains and skullcaps were kept in 4% PFA for an additional 24 h. The fixed meninges, including the dura mater and arachnoid, were carefully dissected from the skullcaps using a stereomicroscope. Fixed brains and dCLNs were subsequently subjected to gradient dehydration using 20% and 30% sucrose solutions and embedded in tissue-plus OCT compound (Sakura, Torrance, CA; Cat# 4583).

The brain segments encompassing the hippocampus and adjacent cerebral cortex were sliced into coronal sections at a thickness of 20 μ m, while the frozen lymph nodes were sectioned into 10- μ m slices using a cryostat (Leica, CM1950, Germany). The sections were then transferred to cryoprotectant (50% glycerol, 50% 0.1 mol/L PBS, pH 7.4) and stored at –20 °C until needed. SVEC4-10 cells were fixed in 4% PFA for 15 min at room temperature, washed with PBS, and subsequently stored at 4 °C until further staining.

Immunofluorescence

Frozen brain sections, lymph node slices, meningeal whole mounts, SVEC4-10 cells, and primary astrocytes on glass coverslips were blocked and permeabilized for one hour at room temperature using a block/stain buffer (0.3% Triton X-100 and 10% bovine serum in PBS). The sections were then incubated with primary antibodies (Table S1) in block/stain buffer overnight at 4 °C, washed three times in PBS, and incubated with secondary antibodies (at a 1:1000 dilution) for 2 h at room temperature. After being washed in PBS and incubated with 4′,6-diamidino-2-phenylindole dihydrochloride (DAPI) at a concentration of 1 μ g/mL in PBS, the sections were coverslipped until images were acquired using a wide-field microscope (DM4000B, Leica) or a confocal microscope (Zeiss LSM710, Germany).

Thioflavin-S staining

Frozen brain sections were stained with 1% Thioflavin-S (Sigma, St. Louis, MO; Cat# 1326–12-1) for 5 min. After rinsing with distilled water, they were differentiated with 70% alcohol for 1 min. The sections were then washed with PBS and mounted with glass coverslips.

Western blotting

Total proteins were extracted from primary astrocytes and mouse hippocampus by incubation in lysis buffer (25 mmol/L Tris pH 7.4, 150 mmol/L NaCl, 1 mmol/L CaCl₂, 1 mmol/L MgCl₂, 0.5% NP-40, and protease inhibitors) for 10 min on ice. The lysates were then centrifuged at 13,000 \times g at 4 °C for 20 min, and the supernatant was collected. Protein concentration was determined using the BCA protein assay (Beyotime Biotechnology, Xiamen, China). Thirty micrograms of protein were mixed with 6 \times loading buffer (Thermo Scientific, Waltham, MA) and boiled at 95 °C for 5 min. The samples were loaded onto 8%–15% gradient gel and transferred to PVDF membranes. The membranes were blocked with 5% non-fat milk for 1 h, and subsequently incubated with primary antibodies (Table S1) overnight at 4 °C. After washing the membranes three times with TBST, they were incubated

with secondary antibodies for 1 h at room temperature. Finally, all bands were washed three times with TBST and imaged using an imaging system (ImageQuant™ LAS 4000 mini, version 1.2).

ELISA

TSP-1 and EAF2 levels in the CSF and hippocampus of mice, as well as in the pellet and supernatant of primary astrocytes, were determined with ELISA commercial kits (Jingmei Co., Ltd. Cat# JM-04106H1, JM-13432M2) following the manufacturer's instructions.

RNA extraction and qRT-PCR

Total RNA was extracted using Trizol reagent (TaKaRa, Kusatsu, Japan), and cDNA was generated using a reverse transcriptase kit (Nanjing Vazyme Biotech Co., Ltd., Cat# R323) following the manufacturer's instructions. qRT-PCR was performed on an ABI 7300 Fast Real-Time PCR System (Applied Biosystems, Foster City, CA) with qRT-PCR SYBR master mix (Vazyme Biotech Co., Ltd. Cat# Q712). mRNA expression level was calculated with the $2^{-\Delta\Delta C_t}$ method as described in a previous report [10]. GAPDH was used as an internal control. The primers used are listed in Table S2.

Tube formation assay

Tube formation assay was performed to assess the effects of recombinant TSP-1 on the tube formation by murine and human LECs in vitro. Matrigel (Coring, NY, USA; Cat# 354243) (10 μ L) was added to the inner wells of 15-well Ibidi μ -slides (Ibidi, Martinsried, Germany; Cat# 81506) and allowed to polymerize for one hour at 37 °C to form a gel-like surface. SVEC4-10 or HLECs in complete culture medium (DMEM, Gibco) with 10% FBS, 100 U/mL penicillin/streptomycin, 1 \times endothelial cell growth supplement containing recombinant TSP-1 (R&D Systems, Minneapolis, MN; Cat# 3074-TH-050), A β_{1-42} (Nanjing Peptide Biotech Ltd. China; Cat# 107761-42-2) or CD36 blocking peptide (Fab Gennix, Frisco, TX; Cat# P-CD36) was seeded onto angiogenesis slides and incubated for 4 h at 37 °C in 5% CO₂. Images were captured and numbers of nodes, sprouts and total tube length were measured and quantified using Image J (NIH, Bethesda, MD).

RNA sequencing

RNA sequencing (RNA-seq) data for meningeal lymphatic endothelial cells from 6-month-old 5 \times FAD male mice and WT mice were obtained from the Gene Expression Omnibus (GEO) database under the accession number GSE245658. Additional bulk RNA-seq data at three different ages (4, 8, and 18 months) in the hippocampus

of 5 \times FAD mice and control mice were sourced from the database with the accession number GSE168137. The count data were utilized for the quantification of gene expression. Normalization and differential expression analysis were performed using the DESeq2 package (version 1.32.0) in R (version 4.3.1). Genes with an adjusted *P*-value less than 0.05 were considered differentially expressed. Principal component analysis (PCA) and hierarchical clustering were conducted to evaluate the overall variance and sample clustering. A specific list of genes, obtained from literature screening, was analyzed to ascertain differential expression across various groups. The expression levels of these genes were extracted and normalized. The gene expression levels in the histogram were normalized using the FPKM value, subtracted by the mean and divided by the standard deviation. Differential expression analysis was conducted for each gene in the list across different groups.

Statistical analysis

Experimenters were blinded to the identity of experimental groups from the time of euthanasia until the end of data collection. Unpaired Student's *t*-test was used to compare differences between two groups. One-way ANOVA with a Tukey *post-hoc* test was used to compare three independent groups. For comparison of multiple factors (e.g., genotype versus treatment), a two-way ANOVA with a Tukey *post-hoc* test was used. A repeated-measures two-way ANOVA with a Tukey *post-hoc* test was applied for repeated observations of multiple factors. Data are presented as mean \pm SEM. Statistical analysis was conducted using R (version 4.3.1) and Prism 8.0 (GraphPad Software, Inc. Boston, MA).

Results

Impaired meningeal lymphatic vessels in 5 \times FAD mice

The meningeal lymphatic vessels which drain brain macromolecule metabolites into the peripheral system, have been reported to be impaired in both aged and AD mice [10, 13, 14]. Consistently, we found significant decreases in the coverage of lymphatic vessels positive for lymphatic vascular endothelial hyaluronan receptor 1 (LYVE-1) and prospero homeobox protein 1 (PROX1), along the transverse sinus (TS) rather than superior sagittal sinus (SSS) of 6.5-month-old 5 \times FAD mice, compared with age-matched WT mice (Fig. 1a, b, d–f). Under physiological conditions, the TS lymphatic vessels consist mostly of a zipper-like junctional pattern of LECs. Insufficient continuous zipper connections are related to impaired lymphatic flow [15, 28]. In the TS lymphatic vessels of 5 \times FAD mice, there was a decrease in tight

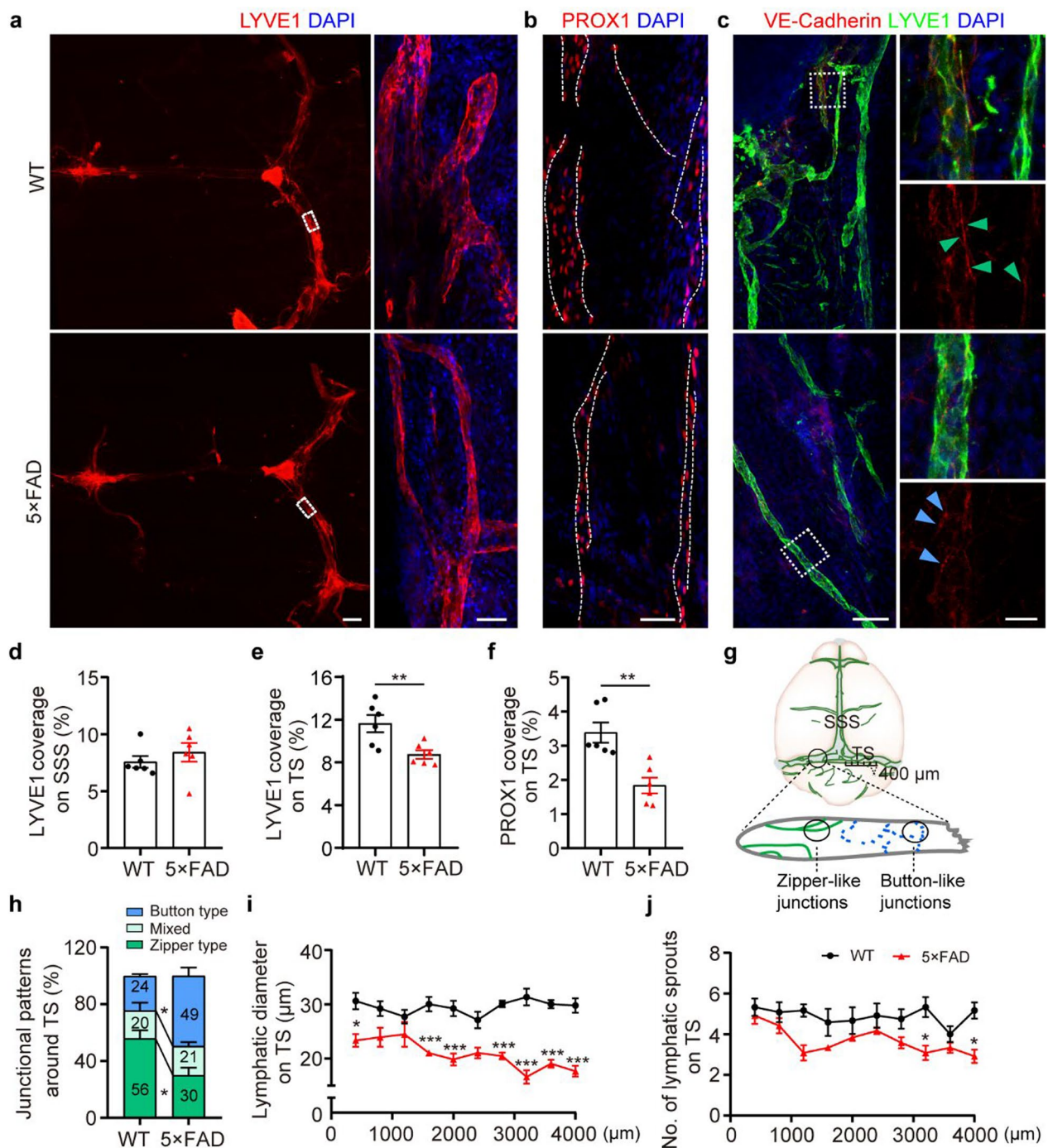


Fig. 1 Impaired meningeal lymphatic plasticity in 5x FAD mice. **a–c** Representative images of LYVE1⁺ (**a**), PROX1⁺ (**b**) and VE-Cadherin⁺ LYVE1⁺ (**c**) meningeal lymphatic vessels in meninges. Scale bars, 800 μm (left) and 50 μm (right) in (**a**), 50 μm in (**b**), 100 μm (left) and 20 μm (right) in (**c**). Arrowheads indicate the dominant junctional pattern. Zipper-like junctions (green arrowheads) are defined as continuous junctions at cell–cell borders of LECs, while button-like junctions (blue arrowheads) are defined as dot-like, discontinuous junctions, roughly parallel linear segments of VE-Cadherin. **d, e** Quantification of LYVE1 coverage area on the TS and superior sagittal sinus (SSS) ($n=6$ per group). **f** Quantification of PROX1⁺ coverage area on the TS ($n=6$ per group). **g, h** Cartoon diagram (**g**) and quantification of VE-Cadherin⁺ lymphatic vessel junctions (**h**). VE-Cadherin immunostaining at least 3.5 μm in length was recognized as zipper junctions, while button-like junctions were defined as a length of 0.5–3.2 μm and a spacing of 2.9 ± 0.3 μm. **i, j** Quantification of the diameters (**i**) and sprout numbers (**j**) of lymphatic extensions in adjacent sections of meningeal lymphatics along TS ($n=6$ per group; bilateral TS per mouse). The lymphatics on the left and right TS were divided into 10 segments (400 μm each), respectively. Data represent the mean \pm SEM; significance was evaluated with unpaired Student's *t*-test (**d–f**) or one-way ANOVA with Tukey *post-hoc* test (**h**) or repeated-measures two-way ANOVA with Tukey *post-hoc* test (**i, j**). * $P < 0.05$, ** $P < 0.01$, *** $P < 0.001$

zipper-like LEC junctions and an increase in button-like LEC junctions compared to those in WT mice (Fig. 1c, g, h). Quantitative analyses also showed reductions in the diameter and the number of sprouts of TS lymphatic vessels in 5×FAD mice, further indicating impaired lymphangiogenesis (Fig. 1i, j).

Activated astrocytes with increased production of TSP-1 in 5×FAD mice

To investigate the underlying mechanism of impaired meningeal lymphangiogenesis in 5×FAD mice, we conducted an RNA-seq analysis of LECs sorted from the meninges of 6-month-old WT and 5×FAD mice (GSE245658). Notably, the classical factors regulating lymphangiogenesis, such as *Vegfc* and *Vegfd*, were not significantly different in meningeal LECs between WT and 5×FAD mice (Fig. S1a-c). This suggested that the soluble cytokines regulating meningeal lymphangiogenesis are not produced by LECs but may originate from brain cells. Consequently, we further evaluated published RNA-sequence data from the hippocampus of WT and 5×FAD mice at 4, 8, and 18 months of age (GSE168137) and screened the literature for factors that regulate lymphangiogenesis. We discovered that *Thbs1*, the gene encoding the protein TSP-1, is age-dependently elevated in the 5×FAD group (Fig. 2a, b, Fig. S2).

TSP-1 is an endogenous inhibitor of lymphangiogenesis, which plays a crucial role in tumor metastasis and transplant outcome [29]. Notably, TSP-1 is a secreted protein primarily produced by astrocytes in the CNS, particularly up-regulated when astrocytes are activated [30, 31]. Consistently, double immunofluorescence revealed that astrocytes surrounding the plaques were activated, with increased TSP-1 expression in the hippocampus of 6.5-month-old 5×FAD mice (Fig. 2c, e, Fig. S3). ELISA further showed high concentrations of TSP-1 in the hippocampus and CSF of 5×FAD mice (Fig. 2f, g). AD mice also exhibited high mRNA expression of TSP-1 receptors CD36 and CD74 in the meningeal lymphatic endothelial cells, compared with WT mice (Fig. 2i). Furthermore, when treated with A β ₁₋₄₂ in vitro, primary astrocytes showed increased expression of TSP-1 in a dose-dependent manner (Fig. 2d, h).

Astrocyte-specific knockdown of TSP-1 enhances meningeal lymphatic vessel plasticity and drainage in 5×FAD mice

To investigate the contribution of astrocyte-derived TSP-1 to impaired meningeal lymphatic drainage in AD, we used an AAV-*Thbs1*-shRNA-mCherry construct (controlled by the GfaABC1D promoter) to selectively knock down *Thbs1* in the hippocampal astrocytes of 5×FAD mice (Fig. 3a). We confirmed reduced TSP-1

levels in the hippocampus and in the CSF of 5×FAD mice, demonstrating the efficacy of the *Thbs1*-shRNA virus (Fig. 3b and Fig. S4a, c). Astrocyte-specific knockdown of *Thbs1* also resulted in an increased diameter of LYVE-1⁺ vessels and continuous zipper-like patterns of LECs in the meningeal tissue (Fig. 3c, d, g, h), as well as a reduction in the accumulation of A β plaques and senescent astrocytes, along with decreased glial activation in the brain parenchyma of 5×FAD mice (Fig. 3e, f, i-k, Fig. S4b, d, e). Furthermore, immunofluorescence staining using monoclonal antibodies against glial fibrillary acidic protein (GFAP) and rabbit IgG antibodies specific for human A β to avoid recognizing endogenously produced mouse IgG1 revealed the presence of non-tissue self-produced antigens or non-specific markers in the dCLNs (Fig. S5a). This supports the notion that these macromolecules are cleared from the brain to the peripheral lymph system [32]. Elevated A β and GFAP signals were observed in the dCLNs of 5×FAD mice following specific knockdown of TSP-1 in hippocampal astrocytes (Fig. S5b, c). As anticipated, the 5×FAD mice with astrocyte-specific knockdown of TSP-1 showed increased number of entries into the novel arm during the Y-maze test, yet the performance in the NOR test was not affected (Fig. S6a-d), suggesting partial mitigation of cognitive impairment. These findings indicate that the astrocyte-specific knockdown of TSP-1 exerts a therapeutic effect on AD model mice by enhancing meningeal lymphatic plasticity and drainage.

TSP-1 aggravates the inhibitory effects of A β on lymphatic vessel formation and plasticity

To confirm the involvement of TSP-1 in lymphatic vessel formation and plasticity, a tube formation assay was initially performed using SVEC4-10 cells, a cell line of LECs [33]. SVEC4-10 cells expressed high levels of lymphatic endothelial markers such as LYVE1, PROX1, and vascular endothelial growth factor receptor 3 (VEGFR3), while exhibiting low expression of vascular endothelial cell markers, including CD31, CD34, and FLI-1, compared with HAECs, a vascular endothelial cell line (Fig. S7a-d). The results indicated that treatment with 200 ng/mL TSP-1 led to reductions in the numbers of nodes and sprouts, as well as the total tube length in SVEC4-10 cells, suggesting that TSP-1 inhibits lymphangiogenesis in vitro (Fig. S8a, b, e). Additionally, previous studies have suggested that meningeal A β deposition may impact the LEC plasticity [13]. In the tube formation assay of SVEC4-10 cells, no significant changes were observed in lymphangiogenesis at lower concentrations of A β ₁₋₄₂ treatment (0, 0.5, and 2.5 μ mol/L). However, the numbers of nodes and sprouts and the total tube length were notably decreased after treatment with 5 μ mol/L A β ₁₋₄₂ (Fig.

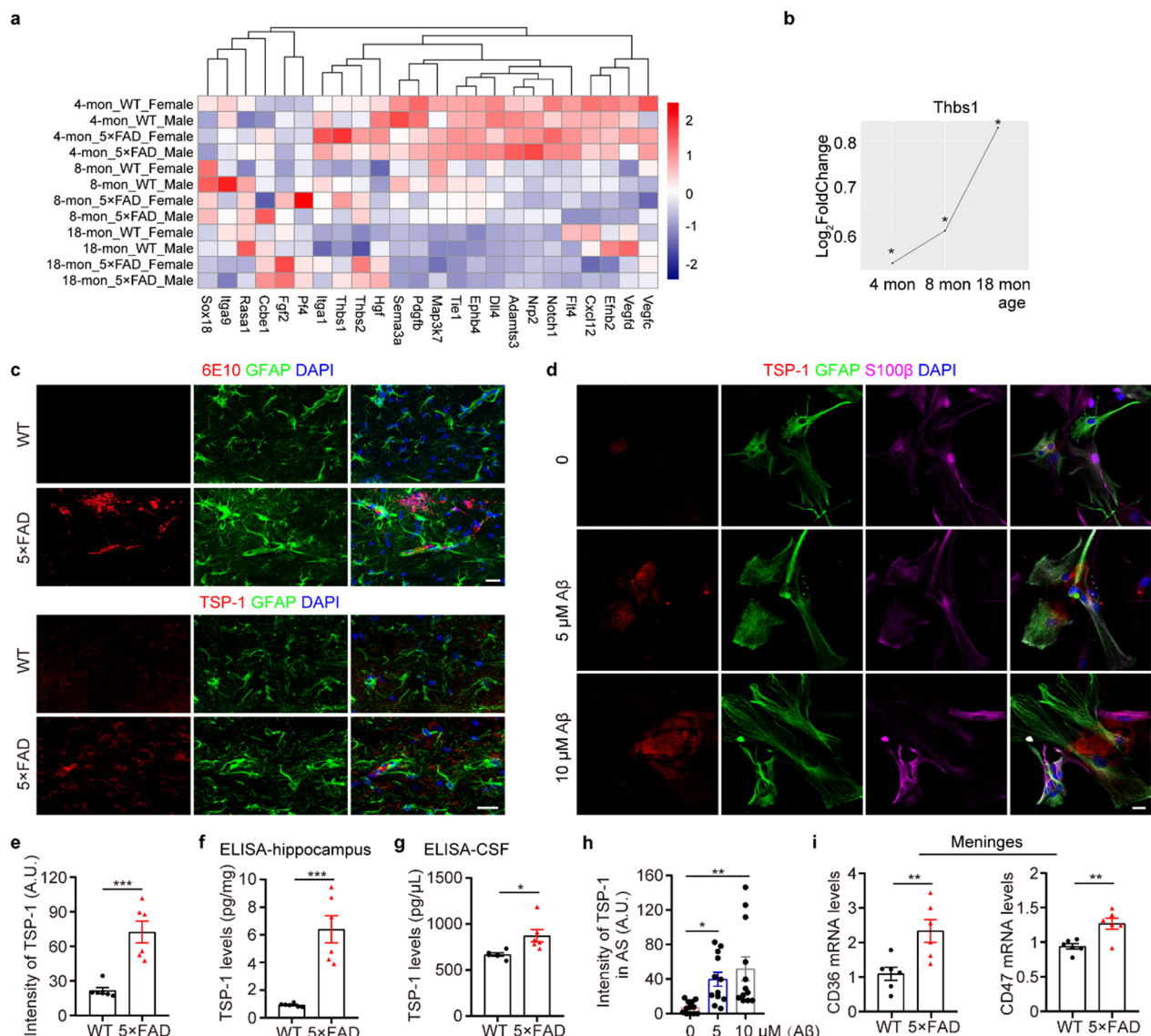


Fig. 2 Increased TSP-1 levels in the hippocampus of 5x FAD mice and cultured astrocytes exposed to Aβ₁₋₄₂. **a** Heat map showing the relative expression level of genes associated with lymphangiogenesis in the hippocampus. **b** The line graph of the log₂ fold change (5x FAD vs. WT) of *Thbs1* expression in the hippocampus at three different ages. **c, e** Representative images of GFAP, 6E10 and TSP-1 staining and quantification of the intensity of TSP-1 in the hippocampus (n = 6 per group). Scale bar, 20 μm (top) and 50 μm (bottom). **d, h** Representative images of astrocytes (labeled with GFAP and S100β) and TSP-1 staining and quantification of the fluorescence intensity of TSP-1 in primary astrocytes (n = 12 per group). Scale bar, 20 μm. **f, g** ELISA assay for TSP-1 levels from the hippocampus (**f**) (n = 6 per group) and CSF samples (**g**) (CSF from two mice combined into one sample, 6 samples per group). **i** Relative mRNA expression of *CD36* and *CD47* in the meninges (n = 6 per group). Data represent the mean ± SEM; significance was evaluated with unpaired Student's *t*-test (**e–g, i**) or one-way ANOVA with Tukey *post-hoc* test (**h**). **P* < 0.05, ***P* < 0.01, ****P* < 0.001

S8c, f). We further investigated whether the combination of lower concentrations of Aβ₁₋₄₂ and TSP-1 has a synergistic inhibitory effect on lymphangiogenesis. The results demonstrated that combined treatment with 2 μmol/L Aβ₁₋₄₂ and 100 ng/mL TSP-1 significantly suppressed tubule formation of the SVEC4-10 cells, compared to

the single-factor treatment described above, which was insufficient to inhibit lymphangiogenesis (Fig. S8d, g).

We further investigated how TSP-1 inhibits lymphatic vessel formation and plasticity. Pretreatment with a CD36-blocking peptide diminished the inhibitory effect of TSP-1 on the lymphangiogenesis of SVEC4-10 cells, as demonstrated in the tube formation assay (Fig. 4a–e).

On the other hand, TSP-1 dose-dependently suppressed the VE–Cadherin zipper-like junctions (Fig. S9a, b). The inhibitory effect of TSP-1 on tube formation and VE–Cadherin continuous junctions was also confirmed in a human-derived lymphatic endothelial cell line HLEC (Fig. S9c–g). Furthermore, the inhibitory effect of TSP-1 at the concentration of 2 $\mu\text{g/mL}$ on these zipper-like junctions was diminished after knockdown of CD47 in SVEC4-10 cells (Fig. S9h–j and Fig. 4f–i). In summary, these in vitro data suggest that TSP-1 inhibits lymphangiogenesis and junction plasticity through interactions with CD36 and CD47, respectively.

Treadmill exercise reduces brain A β load and related pathophysiological changes

Brain A β deposition is a typical hallmark in AD transgenic mice [34]. We assessed whether treadmill exercise could attenuate A β -related brain pathology and cognitive dysfunction in 5 \times FAD mice (Fig. 5a). After one month of treadmill exercise, Thioflavin-S-positive plaques, reactive gliosis, and accumulation of senescent astrocytes were significantly reduced in the hippocampus and the adjacent cortical region of 6.5-month-old 5 \times FAD mice (Fig. S10a–g). Treadmill exercise also had a beneficial effect on the short-term learning and memory of 5 \times FAD mice (Fig. S11a–d). However, exercise intervention did not ameliorate the anxiety-like behavior of 5 \times FAD mice in the EPM test (Fig. S11e, f).

Treadmill exercise increases meningeal lymphatic plasticity and drainage in 5 \times FAD mice

We next determined whether long-term exercise-induced brain A β load decrease is associated with enhanced meningeal lymphatic plasticity. As expected, 6.5-month-old 5 \times FAD mice that received treadmill exercise for one month showed significant increases in the area fraction, diameter, and number of sprouts of meningeal lymphatic vessels, as well as continuous lymphatic junctions (Fig. 5b–h). Furthermore, compared

with the sedentary control group, the treadmill exercise group showed increased A β and GFAP staining in the dCLNs, indicating that exercise facilitates the drainage of brain A β and GFAP from the brain to the peripheral system (Fig. 5i, k, l). These results together revealed that treadmill exercise improves meningeal lymphatic vessel plasticity and drainage under AD-like pathology.

To further confirm this conclusion, in vivo two-photon imaging was used to monitor the dynamic distribution of A β_{1-42} at 1 h post-intrahippocampal administration in the meningeal lymphatic vessels of 6-month-old WT and 5 \times FAD mice that had undergone 10 days of treadmill exercise training (Fig. S12a). As previously reported [35], A β_{1-42} fluorescent signals were detected in the A488-Lyve1-labeled meningeal lymphatic vessels running along the TS. Notably, a comparison of A β_{1-42} –555 drainage through the TS regions at consecutive time points revealed a delayed clearance of the A β tracer in 5 \times FAD mice. The treadmill exercise significantly enhanced the drainage of A β_{1-42} –555 from the meningeal lymphatic vessels in WT mice, and there was a trend toward improvement in AD mice as well (Fig. S12b, c and Additional file Movies 1–4). Consistently, there were increased A β_{1-42} –555 signals in the dCLNs of 5 \times FAD mice after treadmill exercise (Fig. S12d, e). These results verified that exercise promotes the meningeal lymphatic drainage of A β from the brain to the peripheral system.

Treadmill exercise down-regulates TSP-1 expression in astrocytes of 5 \times FAD mice

We examined the expression level of TSP-1 in the hippocampus of 5 \times FAD mice with or without exercise, and found that the upregulated expression of TSP-1 in GFAP-positive astrocytes was reversed by treadmill exercise (Fig. 5j and m). ELISA analysis of the hippocampus confirmed this result (Fig. 5n). ELISA analysis also indicated a significant decrease of TSP-1 level in the CSF after treadmill exercise in 5 \times FAD mice (Fig. 5o). Consistently,

(See figure on next page.)

Fig. 3 Astrocyte-specific *Thbs1* knockdown enhanced meningeal lymphatic vessel plasticity and alleviated accumulation of A β and senescent astrocytes in the hippocampus of 5 \times FAD mice. **a** Schematic of astrocyte-specific *Thbs1* knockdown experiment. Representative images of mCherry staining showing hippocampal injection sites. Scale bar, 500 μm . **b** ELISA assay for TSP-1 levels in the CSF (CSF from two mice combined into one sample, 4 samples per group). **c, d, g, h** Representative images of LYVE1 and VE–Cadherin staining (**d**) and quantification of VE–Cadherin⁺ lymphatic vessel junctions (**c**), LYVE1⁺ area and diameter of LYVE1⁺ vessels (**h**) among TS region (**g**) ($n=6$ per group). Scale bar, 40 μm (top) and 20 μm (bottom). Arrowheads indicate the dominant junctional pattern, zipper junctions (green arrowheads) and button junctions (blue arrowheads). **e, i, j** Representative images of GFAP⁺ senescent astrocytes (white arrowheads) characterized by high expression of p16 (**e**) and quantification of GFAP⁺ area (**i**) and p16⁺ GFAP⁺ astrocytes in the hippocampal lacunosum moleculare layer (LMol) (**j**) ($n=6$ per group). Scale bar, 30 μm . **f, k** Representative images of Thioflavin-S staining and quantification of A β plaque areas in the hippocampus and its surrounding cortical area ($n=6$ per group). Scale bar, 400 μm (top) and 100 μm (bottom). Data are presented as mean \pm SEM; significance was evaluated with two-way ANOVA with Tukey *post-hoc* test (**c, g–k**, * $P < 0.05$, AAV-ctrl-shRNA vs AAV-Thbs1-shRNA, ** $P < 0.01$, *** $P < 0.001$, WT vs 5 \times FAD) or one-way ANOVA with Tukey *post-hoc* test (**b**, * $P < 0.05$, ** $P < 0.01$, *** $P < 0.001$)

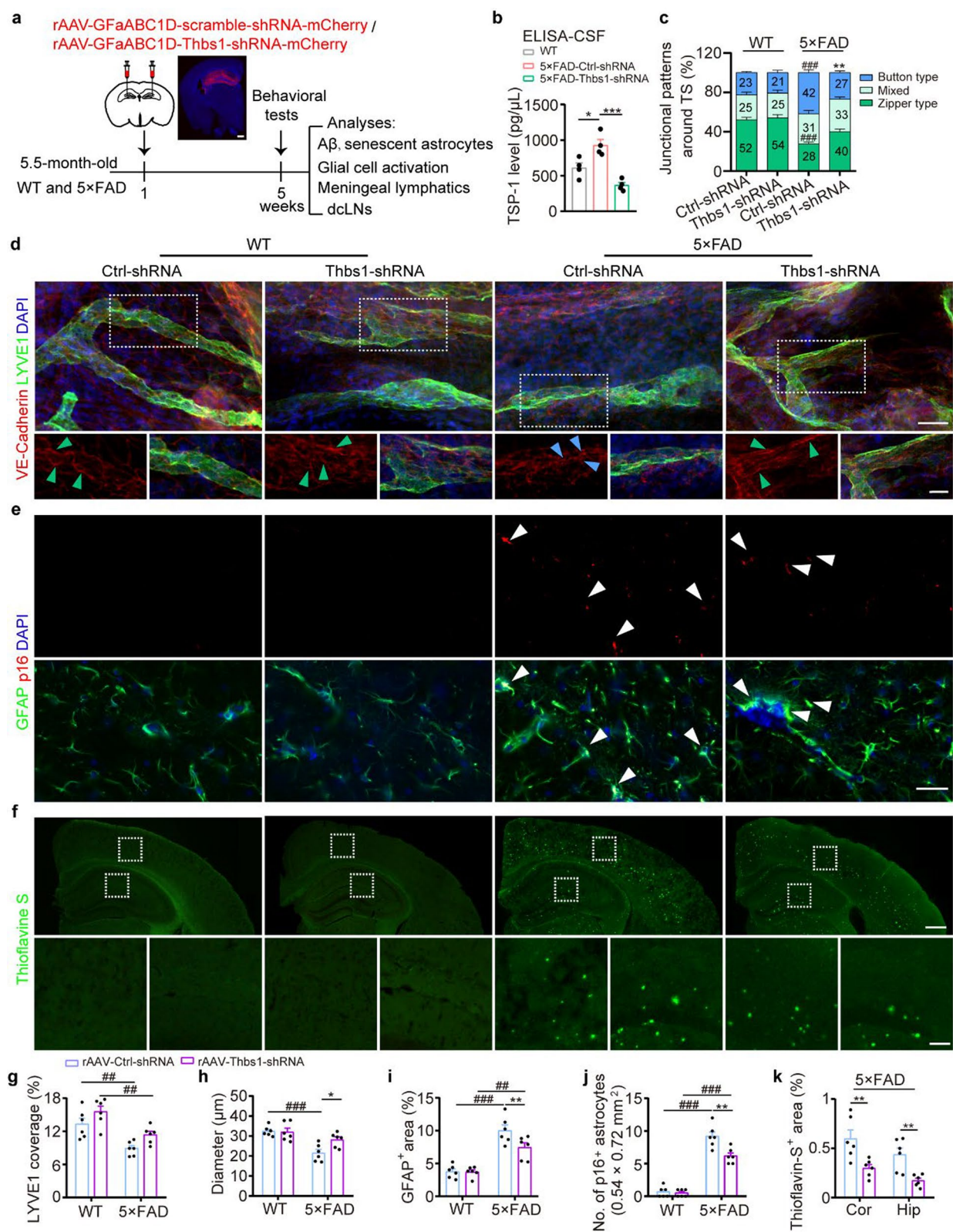


Fig. 3 (See legend on previous page.)

expression of the TSP-1 receptor CD36 in meningeal lymphatic vessels was significantly increased in 5×FAD mice compared to WT mice, but the increase was partially normalized by exercise in 5×FAD mice (Fig. S13a, b).

Besides, the exchange of CSF and interstitial fluid mediated by AQP4 is responsible for the clearance of harmful metabolites from the brain [36]. We observed that, compared with WT littermates, the perivascular localization of astrocytic AQP4 was impaired in the hippocampus of 5×FAD mice, a condition that was reversed by treadmill exercise (Fig. S14a–c). This suggests that treadmill exercise also facilitates AQP4-mediated glymphatic clearance of Aβ. However, the expression levels of APP and its secretases, as well as proteins involved in the transport or degradation of Aβ, were not significantly altered in the hippocampus of WT mice and 5×FAD mice following exercise training (Fig. S15a, b). Collectively, these data suggest that long-term exercise enhances the glymphatic-meningeal lymphatic transport of Aβ, which in turn inhibits the pathological cascades of parenchymal Aβ accumulation, astrocyte activation, TSP1 secretion, and meningeal lymphatic dysfunction, thereby improving the cognitive function of 5×FAD mice.

EAF2 regulating TSP-1 expression in activated astrocytes exposed to Aβ

To further explore how exercise reduces TSP-1 expression, we screened the upstream transcription factors (TFs) of TSP-1 in the hippocampus of WT mice and 5×FAD mice following exercise training, which brought p53 into our focus (Fig. 6a, b). The regulation of TSP-1 by p53 varies across tissues and cells [37–39]. For instance, downregulation of TSP-1 has been shown to increase angiogenesis in the liver of EAF2 knockout mice. However, transfection of EAF2 alone has minimal impact on the TSP-1 promoter [40]. Functional protein association networks analysis indicated that EAF2 has a direct regulatory relationship with p53, but not with TSP-1 (Fig. 6c). Additional evidence was provided by primary astrocytes exposed to varying concentrations of Aβ_{1–42} for 48 h, which demonstrated that the levels of p53, EAF2, and TSP-1 were all elevated at a concentration of 10 μmol/L

(Fig. 6d–g). Furthermore, increased TSP-1 levels in astrocyte cells and their culture medium upon exposure to Aβ_{1–42} were reversed by *Eaf2* knockdown (Fig. 6h–l). Consequently, we hypothesized that EAF2 plays a role in meningeal lymphangiogenesis by modulating TSP-1 levels through its interaction with p53. As anticipated, mRNA expression of p53 was elevated in the hippocampus of 5×FAD mice (Fig. 6b). Additionally, EAF2 was strongly co-localized with activated astrocytes and its expression was increased in the hippocampus of 5×FAD mice compared to WT mice (Fig. 6m, n). Collectively, these findings suggest that Aβ triggers the activation of the EAF2-p53-TSP-1 pathway in astrocytes.

Astrocyte-specific knockdown of EAF2 improves meningeal lymphatic drainage and AD-like pathology in 5×FAD mice

We next investigated whether the drainage of meningeal lymphatic vessels could be enhanced through selective knockdown of astrocytic EAF2. Five-month-old 5×FAD mice were administered with an AAV-Eaf2-shRNA-EGFP construct (controlled by the GfaABC1D promoter) to selectively knock down *Eaf2* in hippocampal astrocytes (Fig. 7a and Fig. S16a, b). Four weeks later, EAF2 levels were also significantly decreased in the CSF of 5×FAD mice (Fig. 7b). These 5×FAD mice, with selective knockdown of the *Eaf2* gene in astrocytes, exhibited improved behavioral performance in the NOR test and Y-maze test (Fig. S17a–d). Furthermore, the hippocampal level of TSP-1 decreased after *Eaf2* knockdown in astrocytes of 5×FAD mice (Fig. 7c–e). Additionally, downregulating EAF2 in astrocytes significantly increased the coverage and diameter of LYVE1⁺ lymphatic vessels and the continuity of the zipper-like patterns of meningeal LECs (Fig. 7f, h and k). This transformation of LEC junction patterns may facilitate Aβ drainage, as evidenced by reductions in Aβ plaques, reactive gliosis, and astrocyte senescence in the hippocampus (Fig. 7i, j, l–o). In line with these findings, Aβ and GFAP levels were higher in the dCLNs compared to control groups (Fig. S18a–c). Collectively, these outcomes suggest that EAF2, derived from activated astrocytes, plays an inhibitory role in meningeal lymphangiogenesis under AD-like pathology.

(See figure on next page.)

Fig. 4 The TSP-1-CD36/CD47 signaling pathway modulates lymphangiogenesis and junction plasticity in vitro, respectively. **a** Schematic of tube formation assay. **b** Representative images of tube formation assay in the SVEC4-10 cells pre-treated with gradient concentrations of exogenous recombinant TSP-1 plus CD36 blocking peptide or control peptide. Scale bar, 100 μm. **c–e** Quantification of the numbers of nodes and sprouts as well as the total tube length in random fields (3.1 × 5.6 mm²), *n* = 8 per group. **f** Schematic of immunofluorescent staining experiment. SVEC4-10 cells were transfected with siRNA-CD47 for 36 h, followed by treatment with 2 μg/mL recombinant TSP-1. **g** Representative images of VE-Cadherin and CD47 staining in the SVEC4-10 cells. Scale bar, 20 μm. **h, i** Quantification of the fluorescence intensity of CD47 and the percentage of zipper-like junctions (*n* = 4 per group). Data are presented as mean ± SEM; significance was evaluated with one-way ANOVA with Tukey *post-hoc* test. **P* < 0.05, ***P* < 0.01, ****P* < 0.001

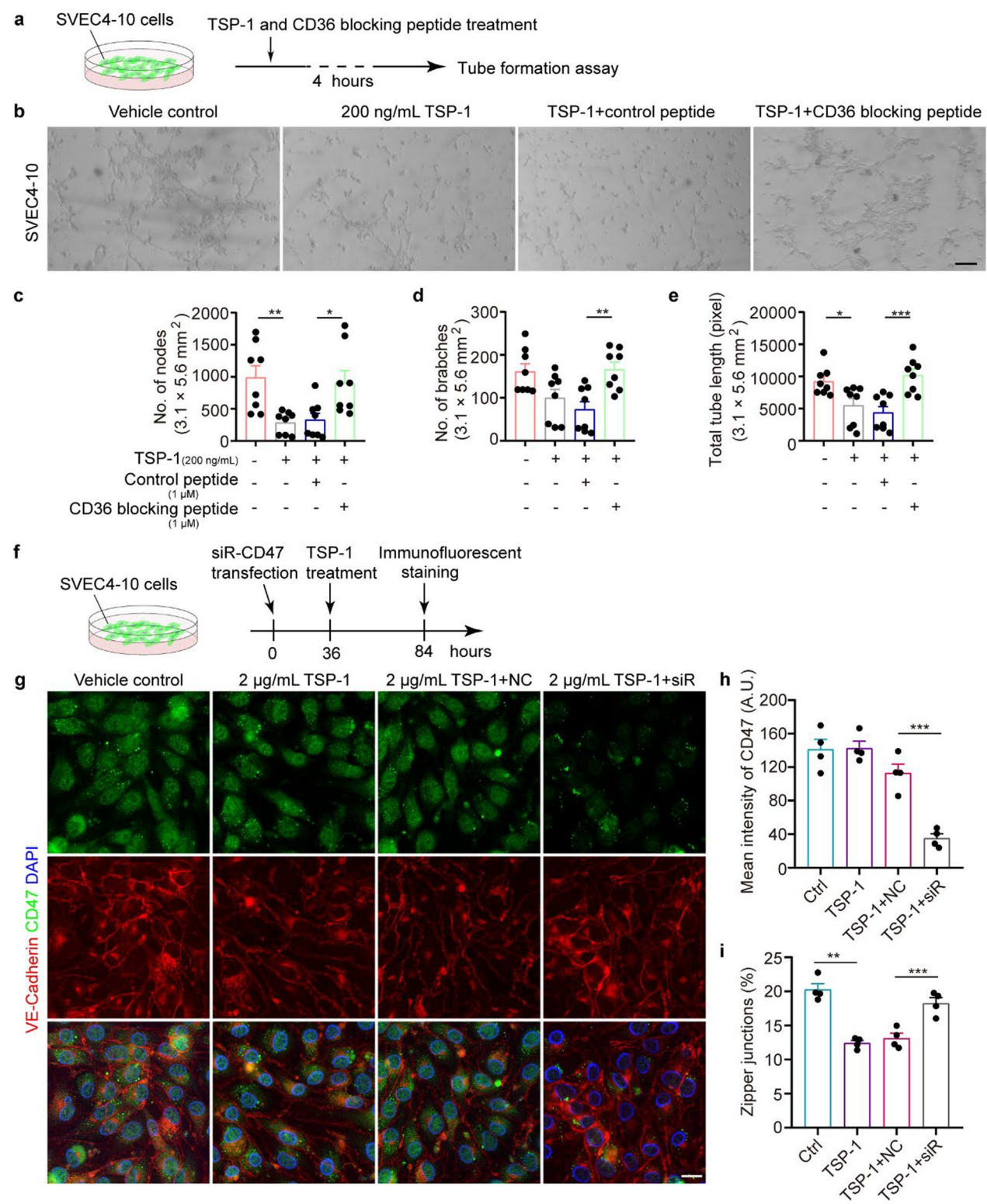


Fig. 4 (See legend on previous page.)

Discussion

In aged or AD mice, impaired meningeal lymphatic drainage is accompanied by decreased macromolecule draining into lymph nodes, as well as cognitive decline [13, 15]. Considering that VEGFC is essential for normal meningeal lymphatic vessel development, overexpression of VEGFC can induce meningeal lymphangiogenesis [16]. Consistently, our previous data also showed a significant increase in the drainage of GFAP into the dCLNs in aged mice after AAV1-CMV-mVEGFC treatment [10]. In the current study, we observed no alterations in the expression of VEGFC in the meninges, but significant upregulation of TSP-1, a secreted protein associated with lymphangiogenesis, in the hippocampus of 6.5-month-old AD mice, compared with WT mice.

The identification of clinical biomarkers for meningeal lymphatic injury is essential for early detection and monitoring of neurodegenerative diseases. Advanced neuroimaging techniques, such as dynamic contrast-enhanced magnetic resonance imaging (MRI) and positron emission tomography, could provide valuable insights into the changes in CSF flow and meningeal lymphatic function [15, 41, 42]. Additionally, CSF biomarkers, encompassing proteins such as A β , tau, and GFAP, as well as lymphatic markers such as podoplanin and LYVE-1, may indicate impaired lymphatic drainage [11, 43]. Beyond these markers, neuroinflammatory cytokines and matrix metalloproteinases, which play roles in blood–brain barrier disruption and lymphatic vessel remodeling, could offer additional evidence of lymphatic dysfunction [44, 45]. Collectively, these biomarkers could improve our capacity to detect and monitor meningeal lymphatic injury in clinical settings. However, this hypothesis requires more evidence. Previous studies have shown that TSP-1 plays a role in peripheral tumor lymphatic metastasis and corneal lymphatic vessel remodeling [29, 46]. However, the expression level of TSP-1 in CNS lymphangiogenesis has not been investigated before. Buee et al. (1992) reported that the distribution of TSPs in the brains of AD patients

was comparable to that in control subjects [47]. In contrast, Son et al. (2015) found downregulation of TSP-1 in cortical samples from individuals with AD [48]. This discrepancy might be attributed to the heterogeneity of astrocyte distribution and the variable disease processes involved in AD.

TSP-1 also acts as a promoter of aging and age-associated diseases. Accumulation of TSP-1 in the extracellular matrix is frequently observed in age-related diseases [49]. In this study, we found that treadmill exercise reduced the expression level of TSP-1 in the brain parenchyma of AD mice. Similarly, RNA sequencing analysis (referring to GSE164401) also revealed a trend of decrease of hippocampal transcriptome level of *Thbs1* in mice injected with plasma from exercising mice, compared with mice receiving control plasma injection. Altogether, these data highlight that exercise interventions alleviate AD pathology by increasing meningeal lymphangiogenesis via TSP-1.

The TSP-1 receptor CD36 serves as a negative regulator of angiogenesis and lymphangiogenesis [50]. In the current study, we further demonstrated that TSP-1 can effectively suppress the proliferation of meningeal lymphatic vessels in vitro by binding to the CD36 receptor on LECs. CD36 has been implicated in maintaining lymphatic vessel integrity, which is associated with obesity and type 2 diabetes models [51]. Deletion of CD36 protects cerebral arteries from the harmful effects of A β _{1–40}, thereby enhancing the cognitive performance of AD model mice [52]. CD47 is another receptor for TSP-1. The TSP-1–CD47 interaction modulates apoptosis of meningeal lymphatic endothelial cells in a subarachnoid hemorrhage model [53]. Elevated levels of TSP-1 impede lymphangiogenesis by activating CD47 in aortic LECs of a mouse model of atherosclerosis [54]. Our findings further indicate that TSP-1–CD47 regulates the junctional pattern of meningeal lymphatic vessels.

EAF2 is preferentially expressed in the CNS during mouse embryonic development [55]. Overexpression of

(See figure on next page.)

Fig. 5 Treadmill exercise increased the plasticity of meningeal lymphatic vessels and reduced TSP-1 levels in 5×FAD mice. **a** Schematic of treadmill training at a 10-degree incline with increasing running speeds (m/min) twice a day for 90 min for 30 days. **b, c** Representative images of PROX1⁺ LYVE1⁺ (**b**) and VE-Cadherin⁺ LYVE1⁺ (**c**) meningeal lymphatic vessels in the TS. Scale bar, 800 μ m (left) and 50 μ m (right) in (**b**), 100 μ m (top) and 20 μ m (bottom) in (**c**). Arrowheads indicate the dominant junctional pattern, zipper-like junctions (green arrowheads) and button-like junctions (blue arrowheads). **d–f** Quantification of LYVE1⁺ (**d**) and PROX1⁺ (**e**) coverage area and VE-Cadherin⁺ lymphatic vessels junctions (**f**) on the TS ($n=6$ per group). **g, h** Quantification of the diameters (**g**) and numbers (**h**) of lymphatic extensions in adjacent sections of meningeal lymphatics along TS ($n=6$ per group; bilateral TS per mouse). **i, k, l** Representative images of A β and GFAP staining in the dCLNs (**i**) and quantification of A β - (**k**) and GFAP-positive (**l**) areas in the dCLNs ($n=6$ per group). Scale bar, 200 μ m (left) and 50 μ m (right). **j, m** Representative images of GFAP and TSP-1 staining (**j**) and quantification of the intensity of TSP-1 in the hippocampus (**m**) ($n=6$ per group). Scale bar, 50 μ m. **n, o** ELISA assay for TSP-1 levels from the hippocampus (**n**) and CSF samples (**o**) (CSF from two mice combined into one sample, 6 samples per group). Data are presented as mean \pm SEM; significance was evaluated with unpaired Student's *t*-test (**d, e, k–o**) or one-way ANOVA with Tukey *post-hoc* test (**f**) or repeated-measures two-way ANOVA with Tukey *post-hoc* test (**g, h**). * $P < 0.05$, ** $P < 0.01$, *** $P < 0.001$

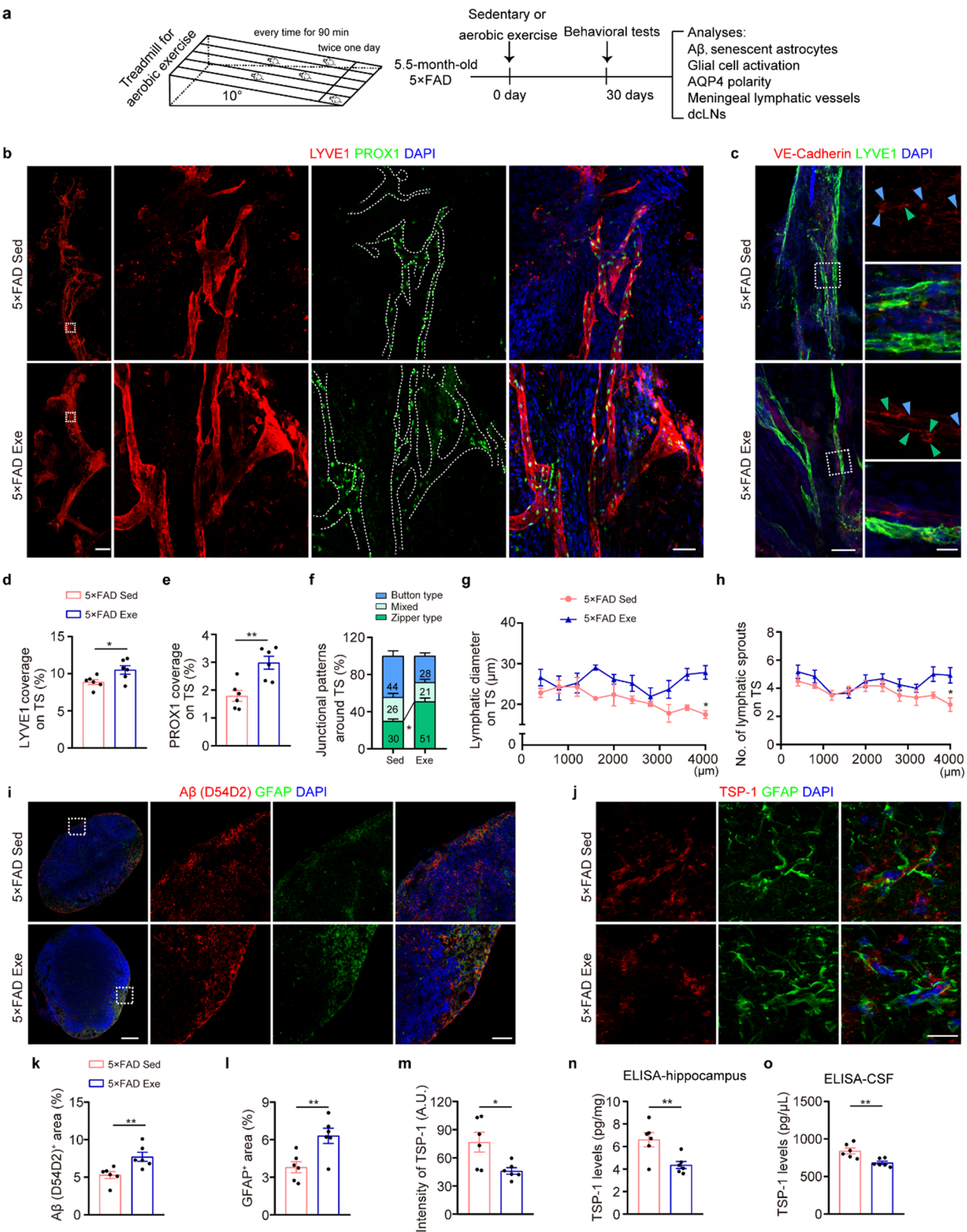


Fig. 5 (See legend on previous page.)

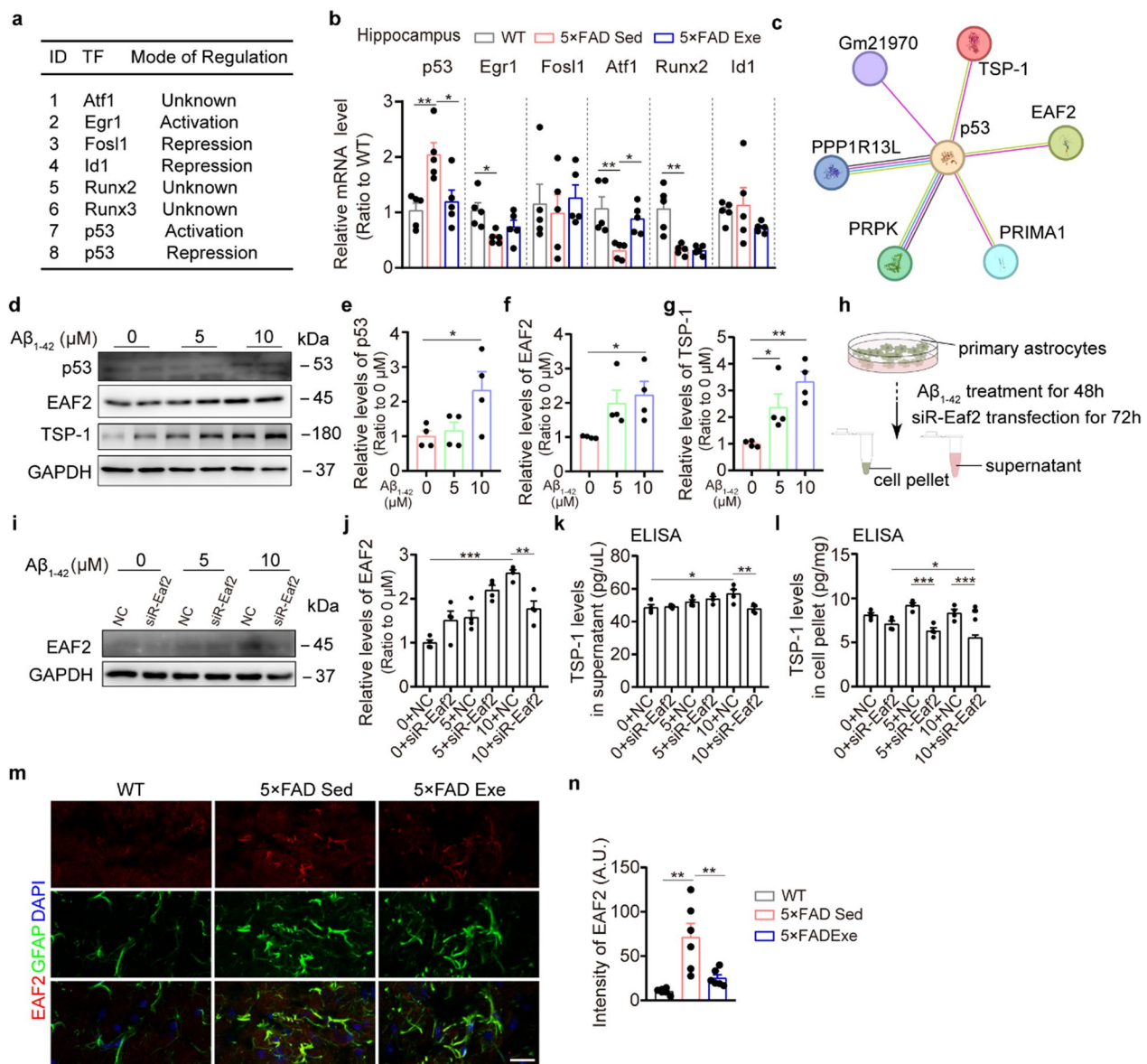


Fig. 6 EAF2 decreased TSP-1 levels through binding to p53. **a** A list of transcription factors (TFs) that regulate *Thbs1*. **b** Relative mRNA expression of upstream regulators of TSP-1 (*p53*, *Egr1*, *Fos1*, *Atf1*, *Runx2*, and *Id1*) in the hippocampus from 6-month-old WT and 5×FAD mice ($n=5$ per group). **c** Functional protein association networks among p53, EAF2 and TSP-1. **d-g** Representative Western blot bands (**d**) and densitometry analysis of p53 (**e**), EAF2 (**f**) and TSP-1 levels (**g**) in the pellet of primary astrocytes treated with gradient AB₁₋₄₂ for 48 h ($n=4$ per group). **h** Schematic of primary astrocytes treated with gradient AB₁₋₄₂ for 48 h followed by knocking down of *Eaf2*. **i, j** Representative Western blot bands (**i**) and densitometry analysis (**j**) of EAF2 levels in the pellet of primary astrocytes treated with gradient AB₁₋₄₂ for 48 h followed by knockdown of *Eaf2* ($n=4$ per group). **k-l** ELISA assay for TSP-1 levels from the supernatant (**k**) and pellet (**l**) of primary astrocytes treated with gradient AB₁₋₄₂ for 48 h followed by knockdown of *Eaf2* ($n=4$ per group). **m** Representative images of EAF2 and GFAP staining and quantification of the fluorescence intensity of EAF2 in the hippocampus. Scale bar, 20 μm, $n=6$ per group. Data represent the mean ± SEM; significance was evaluated with one-way ANOVA with Tukey *post-hoc* test. * $P<0.05$, ** $P<0.01$, *** $P<0.001$

EAF2 induces apoptosis and inhibits cell growth in several peripheral studies [56, 57]. However, its role in the CNS has been scarcely reported. Here we showed that EAF2 expression was upregulated in activated astrocytes of 5×FAD mice, while exercise reversed this increase and

down-regulated its binding partner p53 in 5×FAD mice, thereby promoting the inhibition of TSP-1 by the EAF2-p53 complex. We also demonstrated that knocking down EAF2 in specific astrocytes reduced TSP-1 expression in the brain, which in turn improved meningeal lymphatic

vessel function in AD mice. Collectively, these findings underscore that the EAF2–p53–TSP-1 pathway plays a crucial role in regulating meningeal lymphatic plasticity.

Epidemiological studies have reported that treadmill exercise is a generally applicable form of physical therapy to delay the aging process and improve cognitive function of patients with AD or mild cognitive impairment [58, 59]. However, there is also literature of a different view [60, 61]. Several studies have indicated that treadmill exercise has the potential to reduce A β load in both AD patients and transgenic AD mice [62, 63]. Here, we confirmed that treadmill exercise decreased the parenchymal A β deposition in 6.5-month-old 5 \times FAD mice. A β aggregation and deposition accelerate neuroinflammation and also trigger cellular senescence [3]. Particularly, astrocytes are susceptible to senescence within the CNS [4]. Elimination of senescent glial cells using pharmacological or genetic approaches preserves cognitive function in tau transgenic mouse [5]. In this study, we demonstrated that the enhancement of learning and memory in AD mice through treadmill exercise was accompanied by increased removal of senescent astrocytes from the hippocampus. Previous studies have reported that targeting the clearance of senescent cells, such as cardiomyocytes, pancreatic β cells, and osteocytes, alleviates disease symptoms and slows the aging process [64–66]. Our findings further suggest that elimination of A β and senescent astrocytes may mediate the benefits of treadmill exercise against AD pathology.

A previous study reported that the glymphatic influx in the putamen, as well as the size and flow of meningeal lymphatics, are significantly increased in volunteers after long-term (12 weeks) cycling exercise as assessed by non-invasive MRI [67]. This suggests that sustained physical exercise promotes the flow of putative glymphatic and meningeal lymphatic vessels, thereby enhancing the clearance of brain metabolites in humans. Furthermore, there was no significant difference in lymphatic and meningeal

lymphatic vessel flow before and after a single exercise session. Studies in mice have shown increased CSF influx after 5 weeks of voluntary running-wheel exercise [25]. Similarly, human studies have demonstrated increased middle cerebral artery compliance in volunteers engaged in moderate-to-vigorous recreational aerobic exercise [68]. Based on these findings, it is hypothesized that moderate to high intensity of exercise may significantly contribute to CSF flow and clearance of metabolites from the brain.

Growing evidence suggests that the glymphatic system acts as a functional pathway for the removal of metabolic waste from the brain parenchyma [36]. Voluntary exercise in young mice or aged mice enhances glymphatic function, leading to pro-cognitive effects [24, 25]. Furthermore, our previous study indicated that the improvement of cognitive deficits in APP/PS1 mice through voluntary exercise is dependent on the polarity of astrocytic AQP4 [26]. In the present study, we confirmed that treadmill exercise significantly reduced the activation of astrocytes and improved AQP4 polarity in the hippocampus of 5 \times FAD mice. These findings suggest that the glymphatic system, which is responsible for the clearance of A β , could be an important target for the preventive and therapeutic effects of treadmill exercise on AD.

Furthermore, the meningeal lymphatic system serves as a crucial pathway for the elimination of metabolites and brain antigens from the CSF. Studies have demonstrated that improving the meningeal lymphatic function can improve learning and memory in both aged and AD model mice [13, 14]. Conversely, inhibiting lymphatic drainage in aged mice worsens the accumulation of perivascular senescent astrocytes within the brain parenchyma and exacerbates cognitive behavioral deficits [10]. Additionally, previous research has shown that the cerebral blood flow and CSF flow dynamics significantly increase during exercise in both humans and rodents [25, 69]. In our study, treadmill exercise increased the diameter and the number of sprouts and the continuity

(See figure on next page.)

Fig. 7 Astrocyte-specific *Eaf2* knockdown enhanced meningeal lymphatic vessel plasticity and alleviated accumulation of A β and senescent astrocytes in the hippocampus of 5 \times FAD mice. **a** Schematic of experiments of astrocyte-specific knockdown of *Eaf2*. **a** Representative image of EGFP staining showing hippocampal injection sites. Scale bar, 500 μ m. **b** ELISA assay for EAF2 levels in the CSF (CSF from two mice combined into one sample, 4 samples per group). **c–e** Representative Western blots (**d**) and densitometry analysis of EAF2 (**c**) and TSP-1 (**e**) levels in the hippocampus ($n=6$ per group). **f–h, k** Representative images of LYVE1 and VE-Cadherin staining (**h**) and quantification of VE-Cadherin⁺ lymphatic vessel junctions (**f**), the percentage of LYVE1⁺ area (**g**) and diameter of LYVE1⁺ vessels (**k**) among TS region in the meninges. $n=6$ per group. Scale bars, 40 μ m (top) and 20 μ m (bottom). Arrowheads indicate the dominant junctional pattern, zipper junctions (green arrowheads) and button junctions (blue arrowheads). **i** Representative images of GFAP⁺ senescent astrocytes (white arrowheads) characterized by high expression of p16 in the hippocampal lacunosum moleculare layer (LMol). Scale bar, 30 μ m. **j** Representative images of 6E10 and Iba-1 staining in the hippocampus. Scale bar, 30 μ m. **l, m** Quantification of GFAP⁺ area and GFAP⁺ p16⁺ astrocytes in the LMol ($n=6$ per group). **n, o** Quantification of the percentages of 6E10⁺ and Iba-1⁺ areas in the hippocampus, respectively ($n=6$ per group). Data are presented as mean \pm SEM; significance was evaluated with two-way ANOVA with Tukey *post-hoc* test (**c, e, f, g, k–o**, * $P<0.05$, ** $P<0.01$, *** $P<0.001$, AAV-ctrl-shRNA vs AAV-Thbs1-shRNA, ## $P<0.01$, ### $P<0.001$, WT vs 5 \times FAD) or one-way ANOVA with Tukey *post-hoc* test (**b**, * $P<0.05$, ** $P<0.01$, *** $P<0.001$)

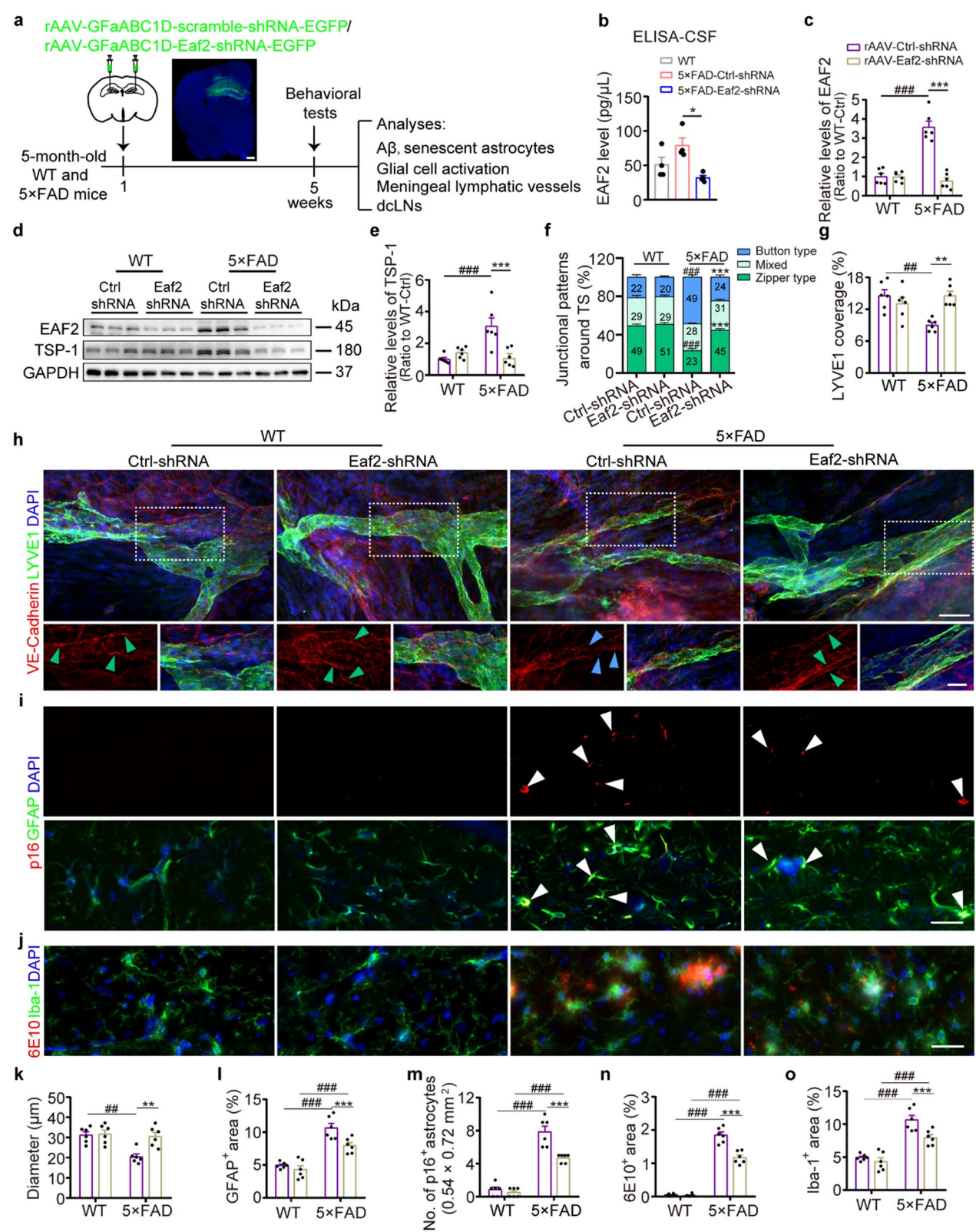


Fig. 7 (See legend on previous page.)

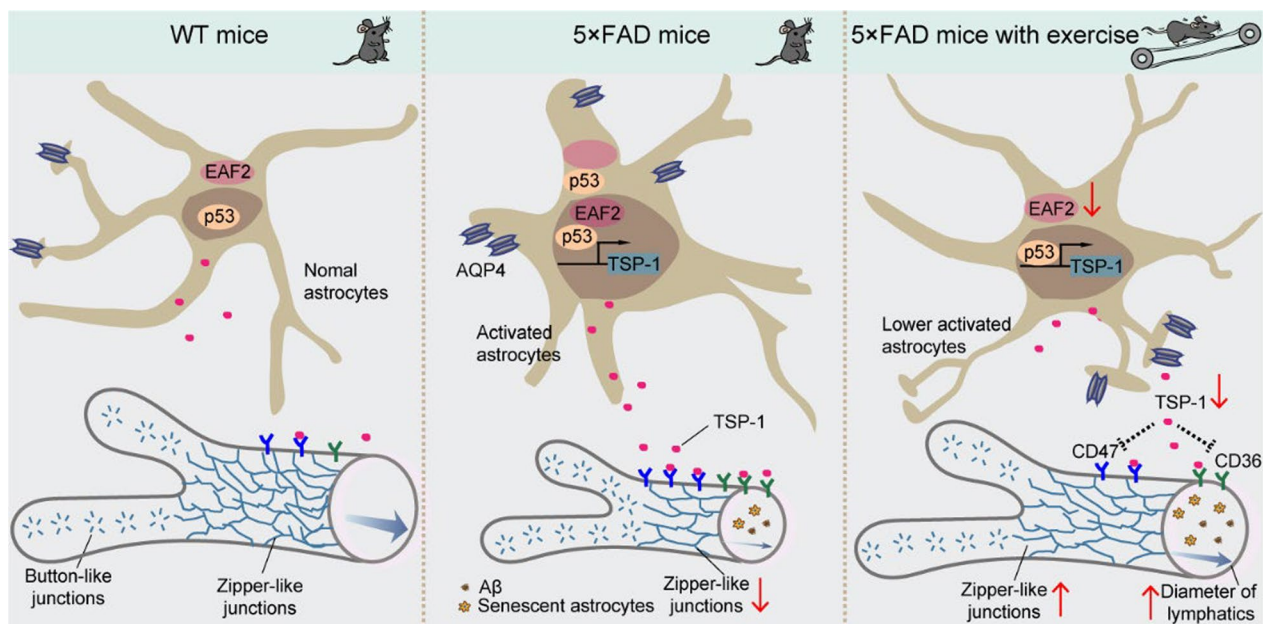


Fig. 8 Illustration of impaired lymphangiogenesis in the AD mouse model, which can be improved by long-term exercise. Exercise increases the zipper-like junctions and the diameter of meningeal lymphatics via down-regulation of the EAF2–p53–TSP-1 pathway, which in turn facilitates drainage of brain A β and reduces astrocyte activation and senescence

of VE–Cadherin junctions in the meningeal lymphatic vessels of AD mice, thereby enhancing their drainage function. This approach could potentially be a promising strategy to improve the clearance of A β , potentially slowing the progression of AD.

It is important to note that the treadmill exercise training was conducted at two time points a day (09:00 and 20:00) to avoid potential effects of circadian rhythms on running. We did not ascertain which time point for treadmill exercise would yield the greatest benefit for the mice. Human studies have indicated that exercise in the morning and the evening have distinct effects on the skeletal muscle molecular clock and nocturnal sleep [70, 71]. The circadian rhythm of the effect of treadmill exercise on the meningeal lymphatic vessels in humans is worthy of further clarification and will maximize the benefits of treadmill exercise, particularly for the elderly or individuals with AD.

Conclusions

The plasticity of meningeal lymphatics has been identified as a significant target for the drainage of metabolites from the brain. Here we demonstrate that TSP-1 produced by activated astrocytes plays a crucial role in the impairment of meningeal lymphangiogenesis in 5x FAD transgenic mice. Astrocyte-specific knockdown of *Thbs1* or *Eaf2* promotes functional meningeal lymphatic vessel

plasticity and mitigates AD-like pathology. Our results also indicate that exercise modulates the lymphangiogenesis and junctional patterns of meningeal lymphatic vessels by down-regulating the reactive astrocyte-related EAF2–p53–TSP-1 pathway (Fig. 8). Our findings suggest a novel mechanism by which exercise improves meningeal lymphatic vessel plasticity, thereby alleviating AD-related pathology.

Abbreviations

AAV	Adeno-associated virus
AD	Alzheimer's disease
AQP4	Aquaporin 4
A β	Amyloid- β
CNS	Central nervous system
CSF	Cerebrospinal fluid
DAPI	4',6-Diamidino-2-phenylindole dihydrochloride
dCLNs	Deep cervical lymph nodes
EAF2	Eleven nineteen lysine rich leukemia-associated factor 2
ELISA	Enzyme-linked immunosorbent assay
EPM	Elevated plus maze
GFAP	Glial fibrillary acidic protein
Iba-1	Ionized calcium-binding adaptor molecule 1
LECs	Lymphatic endothelial cells
LYVE-1	Lymphatic vascular endothelial hyaluronan receptor 1
NOR	Novel object recognition
PROX1	Prospero homeobox protein 1
TFs	Transcription factors
TS	Transverse sinus
TSP-1	Thrombospondin-1
VEGFC	Vascular endothelial growth factor C

Supplementary Information

The online version contains supplementary material available at <https://doi.org/10.1186/s40035-025-00497-2>.

Additional file 1: Figure S1 Expression of classical factors regulating lymphangiogenesis in lymphatic endothelial cells of WT and 5xFAD mice. **Figure S2** Age-dependent changes in factors associated with lymphangiogenesis in the hippocampus among WT and 5xFAD mice. **Figure S3** TSP1 staining in mouse brain regions of WT and 5xFAD mice. **Figure S4** Analysis of microglia and plaques after astrocyte-specific Thbs1 knockdown in the hippocampus of 5xFAD mice. **Figure S5** Astrocyte-specific Thbs1 knockdown increased GFAP and A β levels in the dCLNs of 5xFAD mice. **Figure S6** Astrocyte-specific Thbs1 knockdown alleviated cognitive impairment of 5xFAD mice. **Figure S7** Comparative identification of lymphatic endothelial cell lines of SVEC4-10 and vascular endothelial cell lines of HAECs. **Figure S8** The inhibitory of TSP-1 and A β on lymphatic vessel formation and plasticity via SVEC4-10 cells in vitro. **Figure S9** TSP-1 dose-dependently inhibited VE-Cadherin-formed zipper-like junctions in vitro. **Figure S10** Treadmill exercise alleviated deposition of A β , reactive microglia and astrocyte senescence of 5xFAD mice. **Figure S11** Treadmill exercise alleviated cognitive deficits of 6.5-month-old 5xFAD mice. **Figure S12** Treadmill exercise enhanced meningeal lymphatic vessels function to drain A β of 6.5-month-old 5xFAD mice. **Figure S13** Treadmill exercise down-regulated the elevated CD36 levels in the meninges of 6.5-month-old 5xFAD mice. **Figure S14** Treadmill exercise improved perivascular AQP4 localization of 6.5-month-old 5xFAD mice. **Figure S15** Analysis of treadmill exercise on A β production and clearance-related enzyme of 6.5-month-old 5xFAD mice. **Figure S16** Astrocyte-specific Eaf2 knockdown in the hippocampus of 5xFAD mice. **Figure S17** Astrocyte-specific Eaf2 knockdown alleviated cognitive impairment of 5xFAD mice. **Figure S18** Astrocyte-specific Eaf2 knockdown increased GFAP and A β levels in the dCLNs of 5xFAD mice

Additional file 2: Original western blot bands

Additional file 3: Movie 1. 3D projections of the meningeal lymphatic vessels and A β 1-42-555 of WT sedentary mice by two-photon imaging. Red indicates A β 1-42 and green indicates LYVE-1 in the movies

Additional file 4: Movie 2. 3D projections of the meningeal lymphatic vessels and A β 1-42-555 of WT exercised mice by two-photon imaging. Red indicates A β 1-42 and green indicates LYVE-1 in the movies

Additional file 5: Movie 3. 3D projections of the meningeal lymphatic vessels and A β 1-42-555 of 5xFAD sedentary mice by two-photon imaging. Red indicates A β 1-42 and green indicates LYVE-1 in the movies

Additional file 6: Movie 4. 3D projections of the meningeal lymphatic vessels and A β 1-42-555 of 5xFAD exercised mice by two-photon imaging. Red indicates A β 1-42 and green indicates LYVE-1 in the movies

Acknowledgements

Not applicable.

Author contributions

QL, YC, J C, XH, HF, XL and WY carried out and analyzed immunostaining and behavior tests. LY, YF, MY, YS, and YC carried out biochemistry, in vitro experiments and data analysis. YJ performed cartoon diagrams. WZ and YC carried out and analyzed in vivo two-photon imaging. MX, QL, FD, and YC designed the experiments. MX, QL, CS, JG, and YC wrote and modified the manuscript. All authors read and approved the final manuscript.

Funding

This work was supported by grants from the National Natural Science Foundation of China (82471608, 82204365, 82071199 and 81871117), the Natural Science Foundation of Jiangsu Province (BK20230057), Shandong Postdoctoral Science Foundation (SDCX-ZG-202400044), Shandong Postdoctoral Innovative Talents Program (SDBX2023056) and the Natural Science Foundation of the Jiangsu Higher Education Institutions of China (23KJB310009).

Data availability

All supporting information and data are available in the article and supplementary files.

Declarations

Ethics approval and consent to participate

All animal studies were approved by the Care and Use Committee of Laboratory Animals of Nanjing Medical University (IACUC-1812054).

Consent for publication

Not applicable.

Competing interests

The authors declare that they have no competing interests.

Author details

¹Jiangsu Key Laboratory of Neurodegeneration, Nanjing Medical University, Nanjing 211166, China. ²Institute of Brain Science and Brain-Inspired Research, Shandong First Medical University and Shandong Academy of Medical Sciences, Jinan 250117, China. ³Department of Neurology, Brain Institute, The Affiliated Nanjing Brain Hospital of Nanjing Medical University, Nanjing 210029, China. ⁴Department of Analytical and Testing Center, Nanjing Medical University, Nanjing 211166, China. ⁵Department of Neurology, The First Affiliated Hospital of Nanjing Medical University, Nanjing 210029, China. ⁶Department of Pharmacology, School of Basic Medical Sciences, Fudan University, Shanghai 200032, China. ⁷Department of Anatomy, Nanjing Medical University, Nanjing 211166, China.

Received: 2 January 2025 Accepted: 18 June 2025

Published online: 25 July 2025

References

- Hardy J, Selkoe DJ. The amyloid hypothesis of Alzheimer's disease: progress and problems on the road to therapeutics. *Science*. 2002;297(5580):353–6.
- Selkoe DJ, Hardy J. The amyloid hypothesis of Alzheimer's disease at 25 years. *EMBO Mol Med*. 2016;8(6):595–608.
- Guerrero A, De Strooper B, Arancibia-Carcamo IL. Cellular senescence at the crossroads of inflammation and Alzheimer's disease. *Trends Neurosci*. 2021;44(9):714–27.
- Fletcher-Sanankone E, Kanji S, Tomimatsu N, Di Cristofaro LFM, Kolipara RK, Saha D, et al. Elimination of radiation-induced senescence in the brain tumor microenvironment attenuates glioblastoma recurrence. *Cancer Res*. 2021;81(23):5935–47.
- Bussian TJ, Aziz A, Meyer CF, Swenson BL, van Deursen JM, Baker DJ. Clearance of senescent glial cells prevents tau-dependent pathology and cognitive decline. *Nature*. 2018;562(7728):578–82.
- Xin SH, Tan L, Cao X, Yu JT, Tan L. Clearance of amyloid beta and tau in Alzheimer's disease: from mechanisms to therapy. *Neurotox Res*. 2018;34(3):733–48.
- Louveau A, Smirnov I, Keyes TJ, Eccles JD, Rouhani SJ, Peske JD, et al. Structural and functional features of central nervous system lymphatic vessels. *Nature*. 2015;523(7560):337–41.
- Wang L, Zhang Y, Zhao Y, Marshall C, Wu T, Xiao M. Deep cervical lymph node ligation aggravates AD-like pathology of APP/PS1 mice. *Brain Pathol*. 2019;29(2):176–92.
- Zou W, Pu T, Feng W, Lu M, Zheng Y, Du R, et al. Blocking meningeal lymphatic drainage aggravates Parkinson's disease-like pathology in mice overexpressing mutated α -synuclein. *Transl Neurodegener*. 2019;8:7.
- Li Q, Chen Y, Feng W, Cai J, Gao J, Ge F, et al. Drainage of senescent astrocytes from brain via meningeal lymphatic routes. *Brain Behav Immun*. 2022;103:85–96.
- Li X, Qi L, Yang D, Hao S, Zhang F, Zhu X, et al. Meningeal lymphatic vessels mediate neurotropic viral drainage from the central nervous system. *Nat Neurosci*. 2022;25(5):577–87.
- Hu X, Deng Q, Ma L, Li Q, Chen Y, Liao Y, et al. Meningeal lymphatic vessels regulate brain tumor drainage and immunity. *Cell Res*. 2020;30(3):229–43.

13. Da Mesquita S, Papadopoulos Z, Dykstra T, Brase L, Farias FG, Wall M, et al. Meningeal lymphatics affect microglia responses and anti-A β immunotherapy. *Nature*. 2021;593(7858):255–60.
14. Da Mesquita S, Louveau A, Vaccari A, Smirnov I, Cornelison RC, Kingsmore KM, et al. Functional aspects of meningeal lymphatics in ageing and Alzheimer's disease. *Nature*. 2018;560(7717):185–91.
15. Ahn JH, Cho H, Kim JH, Kim SH, Ham JS, Park I, et al. Meningeal lymphatic vessels at the skull base drain cerebrospinal fluid. *Nature*. 2019;572(7767):62–6.
16. Antila S, Karaman S, Nurmi H, Airavaara M, Voutilainen MH, Mathivet T, et al. Development and plasticity of meningeal lymphatic vessels. *J Exp Med*. 2017;214(12):3645–67.
17. Luo C, Yin H, Gao T, Ma C, Liu J, Zhang T, et al. PEDF inhibits lymphatic metastasis of nasopharyngeal carcinoma as a new lymphangiogenesis inhibitor. *Cell Death Dis*. 2021;12(4):295.
18. Di Benedetto S, Müller L, Wenger E, Düzel S, Pawelec G. Contribution of neuroinflammation and immunity to brain aging and the mitigating effects of physical and cognitive interventions. *Neurosci Biobehav Rev*. 2017;75:114–28.
19. Gleeson M, Bishop NC, Stensel DJ, Lindley MR, Mastana SS, Nimmo MA. The anti-inflammatory effects of exercise: mechanisms and implications for the prevention and treatment of disease. *Nat Rev Immunol*. 2011;11(9):607–15.
20. Choi SH, Bylykhashi E, Chatila ZK, Lee SW, Pulli B, Clemenson GD, et al. Combined adult neurogenesis and BDNF mimic exercise effects on cognition in an Alzheimer's mouse model. *Science*. 2018;361(6406).
21. Zhao G, Liu HL, Zhang H, Tong XJ. Treadmill exercise enhances synaptic plasticity, but does not alter β -amyloid deposition in hippocampi of aged APP/PS1 transgenic mice. *Neuroscience*. 2015;298:357–66.
22. García-Mesa Y, López-Ramos JC, Giménez-Llort L, Revilla S, Guerra R, Gruart A, et al. Physical exercise protects against Alzheimer's disease in 3xTg-AD mice. *J Alzheimers Dis*. 2011;24(3):421–54.
23. Hoffmann K, Sobol NA, Frederiksen KS, Beyer N, Vogel A, Vestergaard K, et al. Moderate-to-high intensity physical exercise in patients with Alzheimer's disease: a randomized controlled trial. *J Alzheimers Dis*. 2016;50(2):443–53.
24. He XF, Liu DX, Zhang Q, Liang FY, Dai GY, Zeng JS, et al. Voluntary exercise promotes glymphatic clearance of amyloid beta and reduces the activation of astrocytes and microglia in aged mice. *Front Mol Neurosci*. 2017;10:144.
25. von Holstein-Rathlou S, Petersen NC, Nedergaard M. Voluntary running enhances glymphatic influx in awake behaving, young mice. *Neurosci Lett*. 2018;662:253–8.
26. Liu Y, Hu PP, Zhai S, Feng WX, Zhang R, Li Q, et al. Aquaporin 4 deficiency eliminates the beneficial effects of voluntary exercise in a mouse model of Alzheimer's disease. *Neural Regen Res*. 2022;17(9):2079–88.
27. Rocchi A, He C. Activating autophagy by aerobic exercise in mice. *J Vis Exp*. 2017(120).
28. Rustenhoven J, Pavlou G, Storck SE, Dykstra T, Du S, Wan Z, et al. Age-related alterations in meningeal immunity drive impaired CNS lymphatic drainage. *J Exp Med*. 2023;220(7).
29. Cursiefen C, Maruyama K, Bock F, Saban D, Sadrai Z, Lawler J, et al. Thrombospondin 1 inhibits inflammatory lymphangiogenesis by CD36 ligation on monocytes. *J Exp Med*. 2011;208(5):1083–92.
30. Dong Z, Zhan T, Sun H, Wang J, Duan G, Zhang Y, et al. Astrocytic ERK/STAT1 signaling contributes to maintenance of stress-related visceral hypersensitivity in rats. *J Pain*. 2022;23(11):1973–88.
31. Tyzack GE, Sitnikov S, Barson D, Adams-Carr KL, Lau NK, Kwok JC, et al. Astrocyte response to motor neuron injury promotes structural synaptic plasticity via STAT3-regulated TSP-1 expression. *Nat Commun*. 2014;5:4294.
32. Günther HS, Henne S, Oehlmann J, Urban J, Pleizier D, Renevier N, et al. GFAP and desmin expression in lymphatic tissues leads to difficulties in distinguishing between glial and stromal cells. *Sci Rep*. 2021;11(1):13322.
33. Park M, Cho KA, Kim YH, Lee KH, Woo SY. Lymphatic endothelial cells promote T lymphocyte migration into lymph nodes under hyperlipidemic conditions. *Biochem Biophys Res Commun*. 2020;525(3):786–92.
34. Masters CL, Bateman R, Blennow K, Rowe CC, Sperling RA, Cummings JL. Alzheimer's disease. *Nat Rev Dis Primers*. 2015;1:15056.
35. Aspelund A, Antila S, Proulx ST, Karlén TV, Karaman S, Detmar M, et al. A dural lymphatic vascular system that drains brain interstitial fluid and macromolecules. *J Exp Med*. 2015;212(7):991–9.
36. Rasmussen MK, Mestre H, Nedergaard M. Fluid transport in the brain. *Physiol Rev*. 2022;102(2):1025–151.
37. Kwak C, Jin RJ, Lee C, Park MS, Lee SE. Thrombospondin-1, vascular endothelial growth factor expression and their relationship with p53 status in prostate cancer and benign prostatic hyperplasia. *BJU Int*. 2002;89(3):303–9.
38. Harada H, Nakagawa K, Saito M, Kohno S, Nagato S, Furukawa K, et al. Introduction of wild-type p53 enhances thrombospondin-1 expression in human glioma cells. *Cancer Lett*. 2003;191(1):109–19.
39. Tokunaga T, Nakamura M, Oshika Y, Tsuchida T, Kazuno M, Fukushima Y, et al. Alterations in tumour suppressor gene p53 correlate with inhibition of thrombospondin-1 gene expression in colon cancer cells. *Virchows Arch*. 1998;433(5):415–8.
40. Su F, Pascal LE, Xiao W, Wang Z. Tumor suppressor U19/EAF2 regulates thrombospondin-1 expression via p53. *Oncogene*. 2010;29(3):421–31.
41. Dobson H, Sharp MM, Cumpsty R, Criswell TP, Wellman T, Finucane C, et al. The perivascular pathways for influx of cerebrospinal fluid are most efficient in the midbrain. *Clin Sci (Lond)*. 2017;131(22):2745–52.
42. Plog BA, Nedergaard M. The glymphatic system in central nervous system health and disease: past, present, and future. *Annu Rev Pathol*. 2018;13:379–94.
43. Xie L, Kang H, Xu Q, Chen MJ, Liao Y, Thiyagarajan M, et al. Sleep drives metabolite clearance from the adult brain. *Science*. 2013;342(6156):373–7.
44. Scalise AA, Kakogiannis N, Zanardi F, Iannelli F, Giannotta M. The blood-brain and gut-vascular barriers: from the perspective of claudins. *Tissue Barriers*. 2021;9(3):1926190.
45. Detry B, Ericum C, Paupert J, Blacher S, Maillard C, Bruyère F, et al. Matrix metalloproteinase-2 governs lymphatic vessel formation as an interstitial collagenase. *Blood*. 2012;119(21):5048–56.
46. Yin Q, Wang PP, Peng R, Zhou H. MiR-19a enhances cell proliferation, migration, and invasiveness through enhancing lymphangiogenesis by targeting thrombospondin-1 in colorectal cancer. *Biochem Cell Biol*. 2019;97(6):731–9.
47. Buée L, Hof PR, Roberts DD, Delacourte A, Morrison JH, Fillit HM. Immunohistochemical identification of thrombospondin in normal human brain and in Alzheimer's disease. *Am J Pathol*. 1992;141(4):783–8.
48. Son SM, Nam DW, Cha MY, Kim KH, Byun J, Ryu H, et al. Thrombospondin-1 prevents amyloid beta-mediated synaptic pathology in Alzheimer's disease. *Neurobiol Aging*. 2015;36(12):3214–27.
49. Isenberg JS, Roberts DD. Thrombospondin-1 in maladaptive aging responses: a concept whose time has come. *Am J Physiol Cell Physiol*. 2020;319(1):C45–c63.
50. Silverstein RL, Febbraio M. CD36, a scavenger receptor involved in immunity, metabolism, angiogenesis, and behavior. *Sci Signal*. 2009;2(72):re3.
51. Cifarelli V, Appak-Baskoy S, Peche VS, Kluzak A, Shew T, Narendran R, et al. Visceral obesity and insulin resistance associate with CD36 deletion in lymphatic endothelial cells. *Nat Commun*. 2021;12(1):3350.
52. Park L, Zhou J, Zhou P, Pistick R, El Jamal S, Younkin L, et al. Innate immunity receptor CD36 promotes cerebral amyloid angiopathy. *Proc Natl Acad Sci U S A*. 2013;110(8):3089–94.
53. Wang X, Zhang A, Yu Q, Wang Z, Wang J, Xu P, et al. Single-cell RNA sequencing and spatial transcriptomics reveal pathogenesis of meningeal lymphatic dysfunction after experimental subarachnoid hemorrhage. *Adv Sci (Weinh)*. 2023;10(21):e2301428.
54. Singla B, Aithbathula RV, Pervaiz N, Kathuria I, Swanson M, Ekuban FA, et al. CD47 activation by thrombospondin-1 in lymphatic endothelial cells suppresses lymphangiogenesis and promotes atherosclerosis. *Arterioscler Thromb Vasc Biol*. 2023;43(7):1234–50.
55. Li M, Wu X, Zhuang F, Jiang S, Jiang M, Liu YH. Expression of murine ELL-associated factor 2 (Eaf2) is developmentally regulated. *Dev Dyn*. 2003;228(2):273–80.
56. Hahn J, Xiao W, Jiang F, Simone F, Thirman MJ, Wang Z. Apoptosis induction and growth suppression by U19/Eaf2 is mediated through its ELL-binding domain. *Prostate*. 2007;67(2):146–53.
57. Qiao Z, Wang D, Hahn J, Ai J, Wang Z. Pirin down-regulates the EAF2/U19 protein and alleviates its growth inhibition in prostate cancer cells. *Prostate*. 2014;74(2):113–20.

58. Yu F, Vock DM, Zhang L, Salisbury D, Nelson NW, Chow LS, et al. Cognitive effects of aerobic exercise in Alzheimer's disease: a pilot randomized controlled trial. *J Alzheimers Dis.* 2021;80(1):233–44.
59. Yu F, Bronas UG, Konety S, Nelson NW, Dysken M, Jack C Jr, et al. Effects of aerobic exercise on cognition and hippocampal volume in Alzheimer's disease: study protocol of a randomized controlled trial (The FIT-AD trial). *Trials.* 2014;15:394.
60. Wolf SA, Kronenberg G, Lehmann K, Blankenship A, Overall R, Staufenbiel M, et al. Cognitive and physical activity differently modulate disease progression in the amyloid precursor protein (APP)-23 model of Alzheimer's disease. *Biol Psychiatry.* 2006;60(12):1314–23.
61. Ke HC, Huang HJ, Liang KC, Hsieh-Li HM. Selective improvement of cognitive function in adult and aged APP/PS1 transgenic mice by continuous non-shock treadmill exercise. *Brain Res.* 2011;1403:1–11.
62. Brown BM, Peiffer JJ, Taddei K, Lui JK, Laws SM, Gupta VB, et al. Physical activity and amyloid- β plasma and brain levels: results from the Australian Imaging, Biomarkers and Lifestyle Study of Ageing. *Mol Psychiatry.* 2013;18(8):875–81.
63. Khodadadi D, Gharakhanlou R, Naghdi N, Salimi M, Azimi M, Shahed A, et al. Treadmill exercise ameliorates spatial learning and memory deficits through improving the clearance of peripheral and central amyloid-beta levels. *Neurochem Res.* 2018;43(8):1561–74.
64. Lewis-McDougall FC, Ruchaya PJ, Domenjo-Vila E, Shin Teoh T, Prata L, Cottle BJ, et al. Aged-senescent cells contribute to impaired heart regeneration. *Aging Cell.* 2019;18(3): e12931.
65. Bahrambeigi S, Yousefi B, Rahimi M, Shafiei-Irannejad V. Metformin; an old antidiabetic drug with new potentials in bone disorders. *Biomed Pharmacother.* 2019;109:1593–601.
66. Geng Q, Gao H, Yang R, Guo K, Miao D. Pyrroloquinoline quinone prevents estrogen deficiency-induced osteoporosis by inhibiting oxidative stress and osteocyte senescence. *Int J Biol Sci.* 2019;15(1):58–68.
67. Yoo RE, Kim JH, Moon HY, Park JY, Cheon S, Shin HS, et al. Long-term physical exercise facilitates putative glymphatic and meningeal lymphatic vessel flow in humans. *Nat Commun.* 2025;16(1):3360.
68. Furby HV, Warnert EA, Marley CJ, Bailey DM, Wise RG. Cardiorespiratory fitness is associated with increased middle cerebral arterial compliance and decreased cerebral blood flow in young healthy adults: a pulsed ASL MRI study. *J Cereb Blood Flow Metab.* 2020;40(9):1879–89.
69. Tarumi T, Yamabe T, Fukuie M, Zhu DC, Zhang R, Ogoh S, et al. Brain blood and cerebrospinal fluid flow dynamics during rhythmic handgrip exercise in young healthy men and women. *J Physiol.* 2021;599(6):1799–813.
70. Yamanaka Y, Hashimoto S, Takasu NN, Tanahashi Y, Nishide SY, Honma S, et al. Morning and evening physical exercise differentially regulate the autonomic nervous system during nocturnal sleep in humans. *Am J Physiol Regul Integr Comp Physiol.* 2015;309(9):R1112–21.
71. Gabriel BM, Zierath JR. Circadian rhythms and exercise - re-setting the clock in metabolic disease. *Nat Rev Endocrinol.* 2019;15(4):197–206.